Reviewer 1:

General:

1. PTRMS calibration
The authors used PTRMS measurements to calculate the amount of pinanediol oxidized by OH radical in order to derive the mass yields of SOA produced. A recent study (Pagonis et al., AMT, 2017) has found that gas-wall partitioning of semi-volatile organics in Teflon tubing and inside the PTRMS could cause significant delays (up to two hours) in instrument response to step-function changes in the concentration of the semi-volatile compounds being measured.
As shown in Fig. 2, the authors in this study may have observed similar PTRMS response to the step-wise increases in the injected pinanediol in the chamber. This observation points to a very important factor that might lead to a large uncertainty in the calculated SOA yields, i.e., PTRMS calibration. The authors are suggested to describe in details how exactly PTRMS sensitivity to pinanediol was determined. If pinanediol standard was used, how was the vapor concentration calculated, and how was the vapor wall loss in the instrument accounted for?

ANSWERS: We determined the PTRMS sensitivity to pinanediol by comparing the PTRMS signals with the pinanediol concentrations inside the chamber. We measured the pinanediol concentration using TD-GCMS. We collected samples by drawing chamber air through Tenax® TA filled glass tubes. We used pinanediol in methylene chloride solution with different pinanediol concentrations as the GCMS calibration standard.

Our sampling setup is different from the study Pagonis et al., AMT, 2017. We used a steel sampling tube and heated the line to 60^{o}C. We wanted to minimize the loss of pinanediol to the sampling tube wall or inside the instrument. We found the PD signals dropped to near to zero immediately after we disconnected the sampling tube from the chamber.

2. Dilution experiments
Although the authors state that rapid gas-wall equilibrium partitioning of pinanediol (10-15 min?) was achieved in the chamber, no evidence could be found throughout of the manuscript. On the other hand, based on what is shown in Figure 2, it seems like there is a slowly decreasing trend in the measured concentration following each pinanediol injection. How did the authors define exactly the time it takes to reach gas-wall equilibrium partitioning?
The authors attribute the missing spike and the slow increase in the pinanediol signal upon a succession of standard injection to the slow equilibration of the PTRMS sampling line. This might also be the reason for the observed PD:AN ratio during the dilution experiment. How long does it take between the PD/AN injection and the onset of dilution? Is it possible that the PTRMS sampling line was far from equilibration with the pinanediol vapor in the sampling air during the entire dilution experiment (or at least the very first few hours)? If this is the case, then the sampling line could possibly act as a constant sink of the pinanediol vapor and the amount evaporated from the wall upon dilution of the chamber might be compensated by that deposited onto the sampling tubing. Have the authors thought about why the PD/AN ratio only started to increase after 5 hours of dilution (or the PD concentration dropped below 2% of the initial

concentration?) This gas-wall partitioning behavior seems very inconsistent with the observation from the heating experiment.

ANSWERS: The 10-15 mins timescale was calculated for SVOCs in the chamber in our previous paper (Ye et al., 2016a), and also observed by Krechmer et al (Krechmer et al., 2016). In Fig. 2, the slow increase was caused by three factors, the injection time (15mins), the chamber mixing time (5-10mins), and the gas wall partitioning equilibration time (10-15mins). These three factors overlapped each other and could not be determined individually. However, we have very strong evidence from both direct observations of H_2SO_4 vapor loss as well as SVOC loss from coated particles, as reported in Ye et al., 2016a, that the intrinsic chamber-wall collisional timescale is 10-15 minutes for compounds with the molecular weights of interest here, including analogues to PD such as oleic acid. Even the differences in timescales (10 min for H2SO4, 15 min for heavier organics) are consistent with theoretical expectations. PD has a higher vapor pressure than most of the SVOCs employed in Ye et al., 2016a, though it is near the high end of the range employed there. It would be very surprising if the PD equilibration timescale were significantly longer and impossible for it to be shorter (the vapor-wall collisional timescale is a lower limit).

We waited around one hour between the PD and acetonitrile (AN) injection and the onset of dilution. If PTRMS sampling line was far from equilibration with the pinanediol vapor in the sampling air, we should observe a very low signal during the injection followed by a steady increase for the hour before we started the dilution. We only observed the continuous decrease after dilution started. Given that both the PD and AN signals both dropped significantly during the dilution experiment (that was the point) and that we are very confident that the AN is a truly passive tracer in both the chamber and the PTRMS and its sampling line, it would take an extraordinary confluence of events for the ratio of the two signals to remain almost perfectly constant without that reflecting a true passive dilution in the chamber itself. It seems not likely that the PTRMS sampling line is far from the equilibration, and thus our conclusion is that the actual gas-phase concentration of PD in the chamber declined during dilution consistent with passive dilution and thus no return flux from PD absorbed or adsorbed to the chamber walls.

That being said, there is an obvious inconsistency in the complete set of observations; nothing can equilibrate without a balance of forward and reverse fluxes, and we have ample evidence of significant PD loss to the chamber walls that non-the-less resulted in a constant PD gas-phase signal proportional to the amount of injected PD. Those are the hallmark signatures of equilibration, as pointed out by Matsunaga and Ziemann. The heating experiments confirm that a large fraction of the PD did indeed partition to the walls. We are fully aware of the inconsistency here, and yet the scientific question of SOA formation from SVOCs in general and PD in specific is pressing. We are still trying to get a good explanation of the different gas-wall partitioning behavior between the dilution and heating experiments. One possible reason may be the evaporation energy of the pinanediol on the chamber wall. The evaporation rate became much higher after heating up the chamber. Then we observed the increase of the pinanediol concentration in the gas phase; however, this does not solve the evident inconsistency at room temperature.

Consequently, we adopted the practical and empirical approach of using the dilution experiments as a controlled test to mimic PD loss via chemical reaction. In this way we are comfortable that we can constrain the total amount of PD oxidized during the experiment, which is absolutely essential for a mass yield determination, but in an abundance of caution we restricted our analysis to the period when at least 20% of the PD remained in the chamber (a factor of 10 more than the point where the dilution experiments showed signs of disequilibrium).

3. Vapor wall loss correction

The authors used a single wall condensation sink (0.063 min^{-1}) measured for SVOCs in the CMU chamber to account for wall losses of vapors across all the volatility range, including LVOCs. While the time for establishing gas-wall equilibrium might be similar (say 10-15 min) for different organic vapors, it has been shown, by many studies, that the amount of organic vapors that reside in the chamber wall phase upon equilibrium depends on the vapor pressure (e.g., Matsunaga and Ziemann, 2010; Zhang et al., 2014, Krechmer et al., 2016). Here by comparing the vapor condensation rate to the wall vs. particles to evaluate the underestimation of SOA yields due to vapor wall loss may bare large uncertainties, as the amount of organic vapors in the wall upon equilibrium partitioning as a dependence of vapor pressure is not accounted for.

ANSWERS: The organics in the SOA are mostly SVOCs, LVOCs and ELVOCs. These organics equivalent saturation concentration in the wall upon equilibrium are more than milligrams/m^3, which is far higher away for the concentration we used in this study. We also used seed concentrations high enough so that the collision timescale to the suspended seeds was more than an order of magnitude higher than the collision timescale with the walls, as discussed in the paper. These two things combined mean that the very large majority of condensable vapors (LVOCs and SVOCs) that encountered the walls should remain there (the equilibrium fraction was < 0.001) but also that most of the SVOCs and all of the LVOCs should have remained on suspended particles for at least a significant portion of the experiment (the other way to think of this is that the steady-state excess saturation between the gas phase and the particles was relatively high during PD oxidation, so the net flux to the suspended particles was close to that of a truly non-volatile constituent. For these reasons we modeled the loss of the SOA vapors to both the chamber walls and the suspended particles as quasi-irreversible. This is definitely an approximation, but our objective is to set up experimental conditions where we are not reliant on uncertain model parameters (i.e. the exact volatility and wall partitioning constants) of condensable species.

4. Accommodation coefficient

The accommodation coefficient is widely used to represent the probability of a vapor molecule sticking onto an organic particle surface. However, the accommodation coefficient used in Equation 3 in this study is essentially an effective accommodation coefficient, as the particle-phase diffusion process needs to be accounted for. Many studies have found that under dry conditions, the phase state of a-pinene SOA is more like semi-solid, implying that the particle-phase diffusion might be the rate limiting step in the overall gas-particle partitioning process. Please comment on the range of accommodation coefficient (0.1-1) chosen here.

ANSWERS: The ELVOCs are extremely low volatility and will stick on the surface when colliding with the particle unless the true mass accommodation coefficient is less than 1. Condensed phase diffusion limitations would cause a substantial activity gradient within the particle, but if the gas-phase activity (the saturation ratio) is >> 1, no condensed-phase activity gradients can significantly influence the microphysics (since the condensed-phase activity is the mole or volume fraction depending on the thermodynamic formulation, for all but very small particles < 10 nm or so with significant curvature). Our conclusion here is that the condensable PD products include a large fraction of ELVOCs, which is also strongly indicated by the new-particle formation experiments at CLOUD.

We have looked and looked and looked for indications of substantial diffusion limitations for SVOC mass transfer between SOA particles, and thus far this has been a rare occurrence. From the literature (Saleh et al., 2013), members of our research team found the accommodation coefficients of alpha-pinene SOA to be >~ 0.2. Other members of our team have explored interactions of suspended SOA populations using isotopically labeled precursors and single-particle measurements (Robinson et al, J Phys Chem, 2013; P. Ye et al., J Phys Chem 2014; Q. Ye et al PNAS 2016; Q Ye et al., Chem, 2018). In no case, for experiments spanning the full range of RH, have we found evidence for substantial delays to vapor exchange between particle populations involving SOA formed from alpha-pinene. While we have not directly studied PD products using this method, we regard the alpha-pinene experiments as a useful analogue. For this reason, we treated two limiting cases, alpha = 0.1 and 1.

Minor:

1. Line 211: Specify how long it takes between the chemical injection into the chamber and the measurement of their concentrations by PTRMS/GCMS. What is the chamber mixing timescale?

ANSWERS: The injection time was 15 mins. Tenex tube samples were collected at 15 mins after the injections were completed. PTRMS was sampling all the time. The chamber mixing time is 5-10 mins.

2. Line 252: Please show evidence for the 'rapid vapor-wall equilibrium' observed in the experiments.

ANSWERS: We observed the rapid change of the SVOC concentration change in the gas phase due to the saturation concentration change caused by the temperature vibration in our previous paper (Ye et al., 2016a)

3. Line 295: Again, specify the time duration between chemical injection and the onset of chamber dilution.

ANSWERS: It was around 1 hour

Reviewer 2:

General comments:

1. What 8 m^3 chamber has a surface area of 12 m^2 (line 105)? This is off by a factor of probably about 2. The smallest surface area to volume ratio is that of a sphere, and a sphere with a volume of 8 m^3 would have a surface area of 19.3 m^2. Likely, any chamber with this volume would have an even larger surface area (and certainly much larger than 12 m^2). Related to this, what is the source of the estimate of 10 g in line 107?

ANSWERS: 12 m^2 is a typo. It should be 24. The chamber is a cubic shape. We used 0.8 g/cm^3 as the density of the Teflon to calculate the 1μm thick Teflon layer mass and got 10 g.

2. How are the data points in Fig. 1 obtained, since in Fig. 2 there is a slightly decreasing trend when the concentrations reach "quasi-steady-state"?

ANSWERS: We averaged the concentrations from the time when the gas concentration got stable to right before the next injection.

3. How do you perform the stepwise injection of the compounds in Fig. 2, i.e. at each injection step does the volume of the chamber change because of constant sampling? Also, you mention the longer evaporation time of the less volatile compound: can you give an estimated timescale?

ANSWERS: We put the mixture the compounds in a flash vaporizer consisting of a stainless steel tip with a machined trough for compounds containing a resistive heating element, all inserted well into the chamber at the end of a stainless steel tube through which we passed purified, heated air. We used the purified air flow to transfer the vapors into the chamber while heating the mixture. The total sampling rate from the chamber was around 5L/min. We used 15L/min air flow to inject the organic mixture for 15 mins. It was around 40 mins between each injection. So the injection and sampling flow were almost balanced. The change of the chamber volume is very small. In this study, the evaporation time of pinanediol was around 10 minutes. We used a low heating output to avoid the thermal decomposition of pinanediol.

4. In the heating experiment (Fig. 3), how much PD do you inject into the chamber at 13^oC in order to get 866 μg m^{-3}? Have you tried to increase temperature to just 22^oC to see if you can get a similar portion of bulk concentration of PD with the ones in Fig. 2? In other words, how can you verify the possibility of pure condensation of PD on the wall or other lines at such a lower temperature? Otherwise, one would think the vapor-wall interaction mechanism is different in heating and dilution experiments.

ANSWERS: We put 20mg pinanediol in the chamber. We tried a series of different amounts of pinanediol. 866 μg/m^3 was in the middle of the gas phase concentrations we

measured. We regarded pure condensation of PD as unlikely since the PD was not saturated in the gas phase. However, it is not obvious at all that this would produce a different result. For "pure condensation" the gas-phase (and condensed-phase) activities would be 1 – the system would be saturated. Consequently, there would be a condensed-phase reservoir with an equilibrium vapor pressure of the PD saturation vapor pressure in the chamber or the lines; this in turn would lead to a significant return flux when the system was dis-equilibrated by dilution. The only substantial difference would be that we would not have been able to add more PD to the gas phase, because it would have been saturated. That is directly contradicted by the data in Figures 1 and 2.

5. In the dilution experiment, you show that PD-wall partition is irreversible above 22% of the initial value, which may be true if the oxidation rate of PD is similar to the dilution rate. So how do you simulate the photo-oxidation of PD? What are the actual values of j_{HONO} and OH level in the chamber? What is the oxidation mechanism used in the simulation: parallel or in series?

ANSWERS: The simulation here was purely experimental. The removal of PD by dilution directly simulates removal of PD by oxidation; there should be no difference to the wall-vapor equilibration because the remaining PD molecules will not "know" how their missing comrades came to vanish - whether down a drain or via oxidation. From the dilution experiment, we found the PD started to release from the chamber wall only after the PD concentration reached 2 μg/m^3. We limited our analysis to the first 1.5 e-folding lifetimes in PD oxidation (we only use the data where the PD concentration is above 8 μg/m^3, 22% of its initial value). For the 2D-VBS simulations we used the constrained (measured) PD removal rate to drive formation of VBS products, again without direct numerical simulation of the gas-phase chemistry.

We injected PD and HONO into the chamber and turned on the UV lights to initiate the oxidation of PD with OH radicals. The OH concentration in these experiments was around 2.4×10^7 molecules/cm^3 for the first hour, then dropped to around 5×10^6 molecules/cm^3 afterwards.

6. If the conclusion in lines 318-320 is correct, why does Fig. 1 not have a y-intercept of 0? Also, how are you accounting for the additional loss you saw in the experiment for Fig. 4?

ANSWERS: The y-intercept is a little bit away from 0 may be due to the large uncertainty of the measurement when PD concentration was low. The decrease of PD was very slow, the loss rate is around 0.05/h. This gave a very small uncertainty when calculating the mass yield. Consequently, we just used the PTR measurement to do the calculations.

7. Around line 372, you are assuming that the condensation sink does not change as more vapor deposits throughout the experiment. How do you justify this assumption, particularly for the boundary layer? The mass transport through the boundary later is

changing throughout the experiment, so the condensation sink of deposited particles also changes.

ANSWERS: We do not assume that the suspended condensation sink is a constant – we measure the suspended particle surface area, correct it for near-surface diffusion (i.e. Fuchs and Sutugen) and calculate the collision frequency of vapors with that suspended surface area. When alpha=1 this is the condensation sink, when alpha < 1 it the condensation sink is slightly larger than alpha x collision frequency (in the transition regime). For the chamber walls, we assume that the condensation sink to the walls is completely limited by diffusion to the chamber walls and that uptake of vapors is quasi-irreversible. McMurry and Grosjean showed decades ago that this will be true so long as the accommodation coefficient of vapors to the walls is larger than roughly 1e-4, and in vapor wall loss experiments we have found no evidence that accommodation is delayed; consequently, vapor transfer to the chamber walls is rate limited by gas-phase diffusion in the quasi laminar boundary layer. Members of our team described this in Trump et al, Aerosol Science and Technology, 2016).

8. Can you clarify the necessity of the correction for delayed condensation? In the caption of Fig. 8, you attribute the delayed condensation to the diffusion time of vapor molecules to the surface of the particles or the wall. Do you mean the gas-phase production rate is too fast compared with the timescale to reach gas-particle-wall equilibrium, so that the instantaneous equilibrium assumption cannot be used at the initial stage?

ANSWERS: The delayed condensation will mostly affect the observed SOA mass in the early stage of the experiments, likely the first 20 mins. During this period, the equilibrium may not be obtained instantaneously.

9. Since you are comparing your experiment to a nucleation experiment in CLOUD (lines 513-520), you should justify your assumption that you used enough seed to suppress nucleation when discussing particle number concentration (line 351).

ANSWERS: This is not an assumption - we measured the suspended number concentration and no new particles appeared. We focused on the chemical compositions observed in this study to the CLOUD experiments. Because we did not observe nucleation in these experiments, the seed particles evidently provided enough surface to prevent the nucleating ELVOCs from building a supersaturation sufficient for nucleation. Members of our team modeled this for the alpha-pinene SOA case, comparing SOA production with CLOUD nucleation, in Chuang et al, ACP, 2017. However, for PD in CLOUD, the nucleation involves sulfuric acid vapor and so we cannot directly compare the nucleation results (we do not know when nucleation "should" or "should not" have occurred in our experiments given the product formation rate, suspended condensation sink, and consequent steady-state supersaturations of nucleating species).

10. How do you distinguish “overall SOA yield” and “instantaneous SOA yield”? It looks like Fig. 9 and Fig. 10 are plots of temporal profile of overall SOA yield.

ANSWERS: The “overall SOA yield” in the manuscript means all SOA yields we observed at different PD initial concentrations. We removed the term “overall” in the revised manuscript. The “instantaneous SOA yield” is the overall SOA yield.

Specific comments:

Line 93: Remove the symbol “‡” in the citation.
Lines 91-94 repeat what is more succinctly said in line 89.
Line 163: I believe the unit is m^3 not m^{-3}.
ANSWERS: We changed those in the manuscript.
Line 178: What type of neutralizer did you use?
ANSWERS: It is Po-210

Lines 199, 265, 269, 271, 306: There should not be a space before °C.
Lines 213 and 220: The period should go after “Fig” not after the number, as is done in the rest of the paper.
ANSWERS: We changed those in the manuscript.

Line 218: Why does it look like the y-intercepts for oxy pinocamphone and PD are not 0?
ANSWERS: The y-intercept is a little bit away from 0 may be due to the large uncertainty of the measurement when PD concentration was low.

Line 228/Fig. 2: The overshoot time for 2-Nonanone appears to be a lot closer to 10 minutes than to 1 min, especially for the data a little after 2 hours.
ANSWERS: We only counted the first peak as the overshoot time in the original manuscript. We changed it to “5 to 10 mins”

Lines 265 and 278-280: These sentences repeat each other but, in line 265, you say “factor of 10 to 30” and in lines 279-280 you just say “30-fold increase.” What happened to the range in the second sentence?

ANSWERS: It should be “factor of 30” in line 265. We changed the wording in the revised manuscript.

Line 283: The PD should be “absorbed into” or “absorbed by” the Teflon walls, not “absorbed in” them.
ANSWERS: We changed it to “absorbed into”

Line 307: Does the ratio decrease before dilution when the concentration is held constant? Otherwise, diffusion into the bulk Teflon does not make sense.

ANSWERS: The ratio also decreased at a similar rate before dilution.

Line 308: This is the wrong Zhang 2015 reference.
ANSWERS: We put in the right reference.

Line 310: There should be a space after "5.5" before "h," as is done in the rest of the paper.
ANSWERS: We changed those in the manuscript.

Line 317: Did you try slowing the rate of dilution even more to see if there was an effect?
ANSWERS: We didn't try a slower dilution rate.

Line 339: "as same as" should be "the same as" or something of that sort.
Line 352: The font is bold.
ANSWERS: We changed those in the manuscript.

Line 352: How do you verify ignoring other dependencies? E.g. the dependence of the wall loss rate on the diameter of the particle.

ANSWERS: The wall loss of particles also depends on the particle size. We added "without considering the size dependence particle wall loss and other effects"

Lines 384 and 386: These lines have odd spaces/indentations.
Line 437: Inconsistent spacing after the equals sign.
Line 474: Be consistent between "oxy-pinocamphone" and "oxy pinocamphone."
Line 466-476: It is better to represent the chemical mechanism in a scheme.
Line 517: OS_C needs a line above it instead of an accent mark.
ANSWERS: We changed those in the manuscript.

Line 535: Where in the supplemental material is this provided?

ANSWERS: It should be "in the following section".

Line 536: You should probably mention this is for $\alpha=1$ and give the justification for choosing this value of α that you give in the figure captions.
Lines 561, 880, and 904: "Teflon," "summary," and "simulation" are misspelled.
Lines S26-S28: It is unclear when you switch to an explanation of method 3.
ANSWERS: We changed those in the manuscript.

Figure 3: Why is there a bump/overshoot in the Pinanediol concentration around 0.1 hours?

ANSWERS: This is probably due to a combination of chamber mixing and the fact that the heating is delivered directly through the walls - it is not unreasonable to expect a surge of material off of the walls during the initial heating shock. However, this is total speculation.

Figures 4 and S1: Why not make these A and B parts of a figure, so that they can be more directly compared?

ANSWERS: This is a good suggestion - we have combined the figures in the revised manuscript.

Figure 5: The SMPS used in this experiment cannot detect nano-particles, so the last sentence about nucleation may not stand.

ANSWERS: We observe growth rates of the accumulation mode (seed) particles and this constrains the growth rates of nucleated particles as well (they will in general be significantly larger). During the active SOA formation period of these experiments the SOA growth rates exceeded 100 nm/h, so any nucleated particles would have grown into our SMPS detection range in 6 min or less, with a very high survival probability. While it is possible that alien nano-spacecraft where zapping the nucleated particles out of the bag before they grew into our detection window, we regard this as sufficiently unlikely to exclude if from our analysis.

Figure 7: Use another color or background for the case $\alpha = 0.1$.
Figure 7: The solid red versus thickly shaded red are very difficult to distinguish, even when viewed in color.
Figure 8: Since you already use red in the figure, it may make more sense to replace the red dashed line with another color.
ANSWERS: We recolored Fig. 7 and 8.

Figure 11: This figure is missing a legend.

ANSWERS: We added a legend.

Figure 12: Missing colorbar for contour lines.

ANSWERS: The contour lines are not colored - they are in the figure for a qualitative representation of the 2D product distribution. The quantitative representation is the sum over O:C (the 1D representation) shown in the lower panel.

Figure 13: I suggest you change “Bulk suspended” to “Particle suspended” in the legend.
Figures S2 and S3: Cn is never defined. Also, in S2, the labels on the blue arrows are sufficiently far away from these arrows to be somewhat confusing.

ANSWERS: We changed those in the manuscript.

Secondary organic aerosol production from pinanediol, a semi-volatile surrogate for first-generation oxidation products of monoterpenes

Penglin Ye[a], Yunliang Zhao, Wayne K. Chuang, Allen L. Robinson, Neil M. Donahue[*]

Center for Atmospheric Particle Studies, Carnegie Mellon University, 5000 Forbes Avenue, Pittsburgh, Pennsylvania 15213, United States

[a]now at: Aerodyne Research Inc, Billerica, MA 01821, USA / Nanjing DiLu Scientific Instrument Inc, Nanjing, 210036, China

Correspondence to: nmd@andrew.cmu.edu

Phone: (412) 268-4415

Abstract

We have investigated the production of secondary organic aerosol (SOA) from pinanediol (PD), a precursor chosen as a semi-volatile surrogate for first-generation oxidation products of monoterpenes. Observations at the CLOUD facility at CERN have shown that oxidation of organic compounds such as PD can be an important contributor to new-particle formation. Here we focus on SOA mass yields and chemical composition from PD photo-oxidation in the CMU smog chamber. To determine the SOA mass yields from this semi-volatile precursor, we had to address partitioning of both the PD and its oxidation products to the chamber walls. After correcting for these losses, we found OA loading dependent SOA mass yields from PD oxidation that ranged between 0.1 and 0.9 for SOA concentrations between 0.02 and 20 μg m^{-3}, these mass yields are 2–3 times larger than typical of much more volatile monoterpenes. The average carbon oxidation state measured with an Aerosol Mass Spectrometer was around -0.7. We modeled the chamber data using a dynamical two-dimensional volatility basis set and found that a significant fraction of the SOA comprises low volatility organic compounds that could drive new-particle formation and growth, which is consistent with the CLOUD observations.

1 Introduction

Particulate matter (PM) in the atmosphere affects human health and life expectancy (Pope et al., 2009) and also influences Earth's climate by absorbing and scattering radiation (Solomon, 2007). Organic compounds constitute a large fraction of that PM, making up around 20–90% of the aerosol mass in the lower troposphere (Kanakidou et al., 2005). Secondary organic aerosol (SOA), formed from oxidation of gas-phase organic compounds in the atmosphere, accounts for a significant fraction of the organic aerosol (OA) in PM (Zhang et al., 2007). In the atmosphere, OA is dynamic due to constant photo-oxidation and associated evolution in thermodynamic properties (Seinfeld and Pandis, 2006; Donahue et al., 2005). However, classical smog-chamber experiments encompass only the early stages of SOA formation, including one generation or at most a few generations of oxidation chemistry (Pandis et al., 1991; Odum et al., 1996a). While those experiments may include some later-generation chemistry, the commonly used two-product model (Odum et al., 1996a) treats the (quasi) first-generation products as effectively non-reactive.

Further oxidation (aging) of SOA may add more functional groups to the carbon backbone, causing the second-generation oxidation products to be even less volatile and more water soluble than the first-generation products, which will also enhance the SOA mass (Donahue et al., 2005). However, ongoing oxidation must eventually fragment products and drive down the SOA mass because the end state of organic oxidation is CO_2 formation (Kroll et al., 2009; Chacon-Madrid et al., 2012; Donahue et al., 2013). There is considerable evidence that the ongoing oxidation chemistry can increase SOA mass and oxidation state, both from smog-chamber experiments (Donahue et al., 2012a; Henry and Donahue, 2012; Qi et al., 2012) and also from flow tubes that simulate many days of oxidation using intense

UV radiation to drive photochemistry (Lambe et al., 2011; Wong et al., 2011; Cubison et al., 2011). The flow-tube results also confirm that oxidation will eventually cause mass loss via fragmentation (Tkacik et al., 2014). The volatility basis set (VBS) was developed to treat this ongoing chemistry by condensing the enormous ensemble of organic compounds involved onto a basis grid described by volatility and the carbon oxidation state (Donahue et al., 2006; Donahue et al., 2011a; Donahue et al., 2012b; Chuang and Donahue, 2016b; Tröstl et al., 2016), with coupling constants constrained by chemical behavior of representative or average compounds (Chacon-Madrid et al., 2012; Donahue et al., 2013).

Bulk SOA aging experiments show that later-generation chemistry will influence SOA properties, but those experiments provide limited mechanistic insight due to the extreme complexity of the chemistry involving multiple generations of multiple products. A complementary approach is to use selected first-generation products from SOA formation to probe second-generation chemistry systematically, and to proceed through representative later-generation products. For example, the known products of α-pinene oxidation include pinonaldehyde, which is one of the most volatile products, and acids such as cis-pinonic acid and pinic acid which are some of the least volatile monomer products (Jang and Kamens, 1999; Jaoui and Kamens, 2001). Smog-chamber experiments at Carnegie Mellon have shown that pinonaldehyde is a modest but significant source of SOA at both high NO (Chacon-Madrid and Donahue, 2011) and low NO (Chacon-Madrid et al., 2013) conditions. Aldehyde chemistry is dominated by OH radical attack on the terminal -CHO moiety, causing fragmentation (Chacon-Madrid et al., 2010), but OH attack along the carbon backbone leads to functionalized products that condense to enhance SOA formation from the first-generation parent α-pinene, with mass yields of roughly 10%

under atmospherically relevant conditions. If the most volatile α-pinene product can enhance SOA production, it stands to reason that less volatile SVOC products would have an even greater effect. Indeed, we have observed very low volatility products from cis-pinonic acid oxidation, such as MBTCA (Müller et al., 2012), but we have not systematically explored the SOA mass yields from first-generation SVOC products. Here we use pinanediol (PD) as a surrogate for semi-volatile first-generation oxidation products of monoterpenes to study this aging chemistry. PD has a volatility similar to cis-pinonic acid ($C^* \sim 300$ μg m^{-3}) but it is commercially available and easier to handle.

One reason that SOA mass yields from SVOCs are not commonly reported is that SVOCs are hard to handle and measure, and mass-yield determinations require accurate values for the amount of oxidized precursor because the mass yield by definition is the ratio of formed SOA to oxidized precursor mass. There are two reasons why this is challenging for SVOCs. First, they are sticky and hard to measure. Second, and more challenging, SVOCs may be lost to Teflon chamber walls (Matsunaga and Ziemann~~‡~~, 2010) and may even return from the chamber walls as oxidation perturbs a putative gas-Teflon equilibrium. This means any measured change in the SVOC concentration, even if an instrument is well characterized, may not reflect the actual amount of oxidized SVOC.

Sorption of SVOCs into Teflon chamber walls has recently become a matter of significant concern. Matsunaga and Ziemann (2010) showed that various organic compounds broadly in the intermediate volatility range (IVOCs, (Donahue et al., 2011a)) appear to sorb reversibly to Teflon chamber walls, and more recent work has confirmed this finding. The fraction of organic vapors left in gas phase appears to depend on the volatility and the molecular structure of the organics, but Matsunaga and Ziemann suggested that IVOCs

partition into a disrupted surface layer of the Teflon as if the Teflon had an equivalent mass of between 2 and 10 mg m^{-3}, depending on molecular structure (for a several cubic meters chamber). As an example, an 8 m^3 chamber has a surface area of ~~12~~ 24 m^2, and if the disrupted Teflon surface layer postulated by Matsunaga and Ziemann were 1 µm thick it would have a volume of 12 x 10^{-6} m^3 and thus a mass of roughly 10 g considering the density of the Teflon is 0.8 g/cm^3; projected to the chamber volume this gives an equivalent mass concentration of roughly 1 g m^{-3}. To have an effective "partitioning mass" of 1-10 mg m^{-3} this material would thus need to have a mass-based activity coefficient of 100-1000 (Trump et al., 2016). This is consistent with weak interactions involving non-polarizable Teflon and also a low degree of interactions among sorbed organics within the walls at the Henry's law, low-concentration limit. However, we must stress that the exact mechanism of organic sorption to Teflon chamber walls remains unclear.

Formatted: Font: (Default) Times New Roman

Formatted: Font: (Default) Times New Roman, Not Bold

More recently, Ye et al. (Ye et al., 2016a) and Krechmer et al. (Krechmer et al., 2016) showed that SVOCs are lost to the Teflon walls steadily, with a time constant of roughly 15 minutes (again for a several cubic-meter chamber). The SVOCs in these studies had 1 < C* < 300 µg m^{-3} and so would be expected to leave only a small fraction ($\ll$ 10%) in the gas phase; this quasi-irreversible loss is thus broadly consistent with the reversible equilibration reported earlier for IVOCs.

We expect PD to partition substantially to the walls of a Teflon chamber. Even 2-decanol showed significant vapor loss (Matsunaga and Ziemann, 2010), and the additional OH group in PD decreases the vapor saturation concentration of PD by around 2.3 decades (Donahue et al., 2011a). This should cause larger mass loss to the chamber walls. In order to get an accurate SOA mass yield from oxidation of PD, we need to determine how much

PD exists in the gas phase vs the chamber walls, and ultimately how much PD reacts during SOA formation experiments.

Another reason we are interested in SOA formation from PD is that it has already been used as a surrogate for the first-generation terpene oxidation products to explore the role of gas-phase aging in new-particle formation, and we wish to compare SOA formation with new-particle formation. The Cosmics Leaving OUtdoor Droplets (CLOUD) facility at CERN is designed to study the effects of cosmic rays on new-particle formation (nucleation and growth) (Kirkby et al., 2011; Duplissy et al., 2016). Early experiments focused on sulfuric acid vapor and different stabilizing species that include the ammonia, amines and oxidation products of organic precursors (Kirkby et al., 2011; Schobesberger et al., 2013; Riccobono et al., 2014). PD was used to mimic first-generation oxidation products of monoterpene formed in the atmosphere (Schobesberger et al., 2013). Specifically the experiments addressed the hypothesis that oxidation of these first-generation products by OH radicals could produce later-generation products with sufficient supersaturation to participate in nucleation (Donahue et al., 2011c). The PD oxidation experiments were among the first to observe highly oxidized, extremely low volatility organic compounds (ELVOCs) (Donahue et al., 2011a), with the original 10 carbon atoms decorated by up to 12 oxygen atoms (Schobesberger et al., 2013; Riccobono et al., 2014). The composition of these highly oxidized organic molecules (HOMs) and possible mechanisms for their formation remains an active research topic (Ehn et al., 2014).

In this study, we focus on SOA formation following oxidation of PD by OH radicals. Our first objective is to extend our understanding of SOA aging via experiments addressing carefully selected first-generation products from common SOA precursors. Our second

objective is to compare the properties of bulk SOA produced at relatively high concentrations (0.3-30 μg m^{-3}) with the PD oxidation products observed condensing onto particles during the CLOUD nucleation experiment. Our third objective is to use PD as a model compound to explore the complications of precursor losses to Teflon walls in smog-chamber SOA formation experiments. We explore the wall sorption of PD by comparing the total amount of PD injected into the chamber to the PD concentration observed in the gas phase. We also investigate the release of sorbed PD from the chamber walls by heating or diluting the chamber. We then calculate the SOA mass yields, accounting for the loss of PD and also the loss of oxidation products to the Teflon chamber walls. Finally, we describe the elemental composition of the formed SOA. We analyze the SOA volatility distribution and oxidation state within the two-dimensional volatility-oxidation set (2D-VBS) and compare the properties of bulk SOA to the ELVOCs observed in CLOUD.

2 Materials and methods

We conducted experiments in the Carnegie Mellon University (CMU) Smog Chamber, a 10 m^{-3} Teflon bag suspended in a temperature-controlled room. The chamber and our methodology have been described extensively in the literature (Hildebrandt et al., 2009). Before each experiment, we cleaned the bag by flushing it with clean, dry air and exposing it to UV irradiation at ~35 °C. We subsequently maintained the chamber at a constant temperature unless otherwise noted.

For the experiments in this paper, we introduced organic compounds into the chamber via a flash vaporizer (Robinson et al., 2013). We used a small, resistive metal heater enclosed in a stainless-steel sheath to evaporate the organics inside the chamber, placing the organics

into an indentation on the stainless-steel surface before inserting the heater into the chamber on the end of a long stainless-steel tube. With a flow of clean, dry dispersion air flowing through the tube for mixing, we power-cycled the heater until the organics completely evaporated. For various experiments, we used *n*-tridecane, 1-tridecene, 2-nonanone, 2-nonanol, oxy-–pinocamphone, and pinanediol (Sigma-Aldrich, 99%). For SOA formation experiments we used ammonium sulfate seed particles ($(NH_4)_2SO_4$, Sigma Aldrich, 99.99%), which we formed by atomizing a 1 g L^{-1} $(NH_4)_2SO_4$ solution in ultrapure deionized water to produce droplets that passed through a diffusion dryer and a Po-210 neutralizer before they entered the chamber. These seed particles served as a condensation sink for condensable vapors in order to reduce vapor wall losses. To form OH radicals during oxidation experiments we added nitrous acid (HONO) to the chamber by bubbling filtered air through a HONO solution for 20 minutes.

We measured gas-phase organic species using both a proton-transfer-reaction mass spectrometer (PTRMS, Ionicon Analytik) and a gas chromatograph/mass spectrometer (GC/MS) (Agilent, 6890 GC/5975 MS) equipped with a thermal desorption and injection system (TDGC/MS, Gerstel, MA) and a capillary column (Agilent HP-5MS, 30 m × 0.25 mm) (Zhao et al., 2014). We maintained the temperature of the PTRMS inlet line at 60-°C to minimize line losses. For the thermal desorption GC measurements, we collected samples by drawing chamber air through Tenax® TA filled glass tubes (Gerstel 6mm OD, 4.5mm ID glass tube filled with ~290 mg of Tenax TA) at a flow rate of 0.5 L min^{-1} for 2 minutes. We tracked the recovery of organics during analysis using C12, C16, C20, C24, C30, C32, C36 deuterated n–alkanes as standards that we spiked into each Tenax tube prior to the thermal desorption.

We measured particle number and volume concentrations inside the chamber using a scanning mobility particle sizer (SMPS, TSI classifier model 3080, CPC model 3772 or 3010). We measured size-resolved and bulk particle composition and mass concentrations with a high-resolution time-of-flight aerosol mass spectrometer (HR-ToF-AMS, Aerodyne Research, Inc.). We operated the HR-ToF-AMS following the common protocol with the vaporizer temperature at 600 °C and electron ionization at 70 eV. We collected mass spectra and particle time-of-flight (pToF) measurements in V-mode, which provides high mass resolution (2000 m/Δm) and excellent transmission efficiency. We analyzed the AMS data using the SQUIRREL V1.53G and PIKA 1.12G.

3 Results and Discussion

3.1 Correction for the loss of the precursors, pinanediol, to the Teflon chamber walls.

Because SVOCs should sorb to the Teflon walls, we expect a portion of PD to be lost after PD was injected into our chamber. To constrain this, we injected equal quantities of six compounds into our chamber simultaneously: PD, oxy-pinocamphone, *n*-tridecane, 1-tridecene, 2-nonanone, and 2-nonanol. The first two are an SVOC and an IVOC, while the last four are VOCs that should have very limited wall partitioning at equilibrium. We then measured the resulting gas-phase concentrations in the chamber using both TD-GC/MS and PTRMS and compared the observed signals to those we expected based on the injected amounts. We finished the injection in 15 mins and collected Tenex tube samples at 15 mins after the injections were completed.

In Fig. 1, we compare the TD-GC/MS measurements with the amounts of organics we injected. We averaged the concentrations from the time when the gas concentration got

Formatted: Indent: First line: 0.14"

Formatted: Font: Not Bold

stable to right before the next injection. The VOCs, *n*-tridecane, 1-tridecene, 2-nonanone and 2-nonanol, all fall along the 1:1 line, demonstrating that they have minimal wall losses and excellent recovery, consistent with our expectations. However, PD and oxy-pinocamphone show large discrepancies between the measured and injected amounts. The recovered gas-phase values show that 43% of the injected oxy--pinocamphone and 86% of the PD were lost; only 14% of the PD remained in the gas phase.

In Fig. 2,~~.~~ we show the results of an experiment where we injected a succession of aliquots of 1-tridecene, 2-nonanone, oxy--pinocamphone and PD into the chamber, with expected stepwise incremental increases of 11 ppbv each, and measured the gas-phase concentrations with a PTRMS. We put the mixture the compounds in a flash vaporizer consisting of a stainless-steel tip with a machined trough for compounds containing a resistive heating element, all inserted well into the chamber at the end of a stainless-steel tube through which we passed purified, heated air. We used the purified air flow to transfer the vapors into the chamber while heating the mixture. We observed that the PTRMS signal stabilized after each injection, and each injection with the same amount of organics resulted in a similar step-wise vapor concentration increase. The two VOCs, 1-tridecene and 2-nonanone, both showed concentration increases consistent with expectations. The PTRMS sensitivity to nonanone is higher than its sensitivity to 1-tridecene, and so the signal to noise is substantially higher. The 2-nonanone shows nearly square-wave response with a brief (~ -5 to 10 mins~~1 min~~) overshoot related to the chamber mixing timescale, and the 1-tridecene signal displayed the same behavior. Oxy--pinocamphone and PD show lower than expected stepwise increases in concentration with a longer rise time. The step-wise increases for oxy--pinocamphone and PD are consistent with near constant wall-loss factors

Formatted: Font: Bold

Formatted: Font: (Default) Times New Roman, Not Bold

Formatted: Font: (Default) Times New Roman, Not Bold

Formatted: Font: (Default) Times New Roman, Not Bold

Formatted: Font: (Default) Times New Roman

in the concentration range in this study, but the signals are not consistent with instantaneous evaporation and subsequent wall partitioning. If that was the case we would expect a large initial spike similar and equal in magnitude to the spike in 2-nonanone (i.e. we would expect the full 11 ppb to appear initially in the gas phase); we would then expect the SVOC signal to drop to an equilibrium value on the equilibrium timescale for wall interactions – 10-15 minutes for our chamber (Ye et al., 2016a), as observed by Krechmer et al using a core-flow inlet CIMS and nitrate chemical ionization (Krechmer et al., 2016). The slow increase in signal we observe may be the convolution of two effects: less than instantaneous evaporation from the flash vaporizer for the SVOCs and slow equilibration of the PTRMS sampling line. Regardless, the signals in the PTRMS stabilize to values consistent with the TD-GC/MS results; these experiments are both consistent with relatively rapid, reversible equilibration of SVOCs (represented by the PD) and IVOCs (represented by the oxy-pinocamphone) between the gases and the Teflon chamber walls.

In order to calculate SOA mass yields, we must determine the amount of precursor oxidized based on the change in precursor signals (e.g. the gas-phase PTRMS measurements). This is straightforward for a VOC with minimal wall interactions, but for the SVOCs we must account for their significant interaction with the Teflon walls. It is not sufficient to simply measure the change in the gas-phase PD concentration, because of the apparently rapid equilibration suggested by the theory put forward by Matsunaga and Ziemann and supported by ~~our wall-loss experiments~~the rapid change of the SVOC concentration change in the gas phase due to the saturation concentration change caused by the temperature vibration in our previous paper (Ye et al., 2016a). If PD were in equilibrium with the walls there would be a substantial source of PD to the gas phase from the Teflon walls as PD was

lost from the gas phase due to oxidization or any other sink. Simply put, the results suggest that, at equilibrium, for every 10 units of PD in the gas phase, roughly 100 units are sorbed in or on the Teflon walls. Therefore, removal of a small amount from the gas phase (say 1 unit) should result in replenishment of 90% by the walls to maintain the equilibrium. Consequently, if we observe a decrease of 1 unit of PD vapor, that implies that 10 units are actually lost from the gas phase since the evaporation of PD from the Teflon walls re-establish the equilibrium. This, obviously, has large implications for the calculated SOA mass yields above and beyond any possible wall losses for products of the PD oxidation.

We use two methods, heating and isothermal dilution, to test whether the Teflon chamber walls in fact serve as an accessible reservoir of PD. Increasing the chamber temperature raises the saturation concentration of PD and thus decreases the activity of PD vapors. Heating by 30 ºC should raise the saturation concentration of PD by a factor of ~~10 to~~ 30 and lower the gas-phase activity (the concentration divided by the saturation concentration) by the same factor. Some PD sorbed to the Teflon should then evaporate to lower the condensed-phase activity. To test this, we injected 866 μg m^{-3} (118 ppbv, the middle value we measured to make sure it is not saturated in the gas phase) of PD vapor into the chamber at 13 ºC and subsequently increased the chamber temperature to 44 ºC. As shown in Fig. 3, the PD vapor concentration measured by the PTRMS increased rapidly after heating and reached a steady value after the temperature stabilized at 44 ºC. The concentration rose by a factor of 2.5-3. To be certain that desorption from the walls was the only possible source, we also monitored the suspended aerosol mass using an HR-AMS. The total organic mass in particles was around 5 μg m^{-3}, far less than the increase of the PD vapor concentration. Particle evaporation thus contributed negligibly to the increase of PD vapors; therefore, the

PD adsorbed or absorbed by the Teflon chamber walls was the only possible source of the increased gas-phase burden.

Increasing temperature by 30 ºC should increase the saturation concentration (C^*) of PD by roughly a factor of 30 (May et al., 2012). All else being equal, this should cause a 30-fold increase in the activity ratio of the sorbed PD to the gas-phase PD and thus drive a large return flux to the gas phase, with the equilibrium vapor fraction increasing from 13% to around 80%. This is consistent with our observations though we observe a factor of 2-3 less than this simple calculation would suggest. However, if PD is absorbed into the Teflon walls, it is likely that the activity coefficient of the PD in Teflon walls would drop substantially upon heating, so this would allow the activities to equilibrate with a smaller net change in absolute concentration. Acknowledging these large uncertainties, the heating experiment is broadly consistent with the postulated reversible equilibration of PD between the gas-phase and the Teflon chamber walls.

Our SOA formation experiments are isothermal, but during the experiments the gas-phase PD concentration (and thus activity) drops due to oxidation. To reproduce these conditions, we used isothermal dilution to mimic the PD loss during SOA formation. We maintained the chamber temperature at 22 ºC and injected PD along with acetonitrile into the chamber, and then measured their concentration ratio using the PTRMS. We used acetonitrile as a passive tracer because it is highly volatile, should not have wall losses, and it is readily measured with the PTRMS. In one hour aAfter injecting PD and acetonitrile into the chamber, we turned on a slow flow of dilution air, initially at a rate of 100 Lpm (1% min^{-1}) and later at a rate of 300 Lpm (3% min^{-1}). These rates roughly bracket the loss rate of PD via OH oxidation in our SOA formation experiments. We tracked the ratio of PD to

acetonitrile. If the PD sorbed to the Teflon chamber wall were released continuously because it was in (a necessarily reversible) equilibrium, the PD concentration should fall more slowly than acetonitrile, and the ratio of PD to acetonitrile should rise steadily. The bottom plot in Fig. 4 ~~We~~ shows a simulation of the expected signals ~~in Fig. S1~~. As ~~, we~~ shown in the top plot ~~in Fig. 4~~, the concentrations of both PD and acetonitrile steadily decreased after we started to flush the chamber. However, we did not observe any increase in the PD to acetonitrile ratio; instead, the ratio remained almost constant, and even showed a slight decrease. This suggests that PD does not return to the gas phase from the Teflon walls at 22 ~~-~~°C, but instead still shows a modest loss to the chamber walls. This indicates slow diffusion into the bulk Teflon, and is inconsistent with the observations in Zhang et al (Zhang et al., 2015b). ~~(Zhang et al., 2015).~~

Formatted: Font: Times New Roman, 12 pt

During the dilution experiments, only after the PD concentration reached 2 μg m^{-3} (2% of the initial concentration), 5.5 h after we started dilution, did the ratio of PD to acetonitrile start to increase. This confirms that PD can return to the gas phase from the chamber walls even during isothermal dilution (or any other isothermal loss from the gas phase), but only after substantial depletion of gas-phase concentrations of PD. Thus, while reversible partitioning to the walls is the most straightforward explanation for the losses of PD we have presented, and even the results of chamber heating are broadly consistent with this explanation, we see no sign of reversibility under the conditions of our SOA formation experiments. This is a paradox, for which we have no explanation.

Therefore, based on the empirical evidence we conclude that the measured decrease in PD from PTRMS during SOA formation experiments is equal to the amount of PD oxidation, and that no further correction for wall equilibration is necessary. There is no reason for the

PD to "know" whether its gas-phase concentration is decreasing because of reaction or isothermal dilution, and so we conclude that the dilution experiment accurately simulates the PD response to reactive loss. However, as a precaution against return flux after substantial PD depletion, we shall limit our analysis to the first 1.5 e-folding lifetimes in PD oxidation (we only use the data where the PD concentration is above 22% of its initial value).

3.2 Correction for particle wall loss.

We conducted experiments to measure the SOA production from oxidation of PD by OH radicals generated via HONO photolysis at five different initial PD concentrations: 1, 2, 4, 5, and 6 ppbv. We used equation 1 to calculate SOA mass yields (*Y*).

$$Y = \frac{C_{SOA}}{\Delta C_{PD}} \quad (1)$$

where C_{SOA} is the measured mass concentration of SOA, and ΔC_{PD} is the mass concentration of the reacted PD. We measured the PD concentration using PTRMS with a unique mass fragment, *m/z*=135, and then calculated the ΔC_{PD}. As we have discussed, we do not correct the measured concentration change in PD for any interaction with the chamber walls. However, in order to calculate the C_{SOA}, we must also account for wall losses of both particles and the condensable SOA products.

We employed three traditional methods to correct the particle wall loss, based on the assumption that particles deposited to the chamber walls function thea~~s~~ same as the suspended particles for the SOA condensation. The corrected SOA production, C_{SOA}, is determined by the ratio of suspended SOA (C_{SOA}^{sus}) to suspended ammonium sulfate seed

(C_{seed}^{sus}) and the initial concentration of ammonium-sulfate seed particles at time 0 h ($C_{seed}^{sus}(t=0)$), as shown in equation 2 (Hildebrandt et al., 2009).

$$C_{SOA}(t) = \frac{C_{SOA}^{sus}(t)}{C_{seed}^{sus}(t)} C_{seed}^{sus}(t=0) \quad (2)$$

The essential term is the SOA to seed ratio, $\frac{C_{SOA}^{sus}(t)}{C_{seed}^{sus}(t)}$. We calculated this ratio directly from the organic and seed (sulfate + ammonium) concentrations measured by the HR-AMS (method 1). We also used the SMPS data. We determined the $C_{seed}^{sus}(t)$ by applying an exponential function to fit the measured decay of the pure ammonium-sulfate seeds before photo-oxidation and then extrapolating that decay for the duration of each experiment (method 2). We also calculated $C_{seed}^{sus}(t)$ by scaling the total particle number concentration (method 3). Because both coagulation and nucleation were minimal during the experiments, we can correct for particle wall losses based on either mass or number loss. $C_{seed}^{sus}(t)$ is proportional to the total suspended particle number concentration. We demonstrate method 2 and 3 in Fig. S12. We calculated $C_{SOA}^{sus}(t)$ as the difference between the total particle mass and the $C_{seed}^{sus}(t)$ after correcting with the SOA density, 1.4 g cm^{-3}, which we calculated following the method of Nakao et al. (Nakao et al., 2013). As shown in Fig. S23, the SOA to seed ratios from these three methods agree to within roughly 20%. Consequently, we focused on the HR-AMS data (method 1) to perform the particle wall-loss correction. We demonstrate one example of the temporal depletion of PD and SOA formation in Fig. S34. Around 80% of PD reacted in the first hour. As mentioned previously, we excluded all data where the PD concentration was less than 22% of its initial value from the analysis; those data are plotted in gray.

Formatted: Font: Not Bold

3.3 Correction for vapor wall loss.

In addition to correcting for the loss of SOA as suspended particles, we also determine the amount of condensable SOA vapors that condense directly to the Teflon chamber walls after PD oxidation. This also reduces the observed SOA mass (Ye et al., 2016a; Krechmer et al., 2016). If the condensing species are functionally non-volatile (their saturation ratios are much larger than their particle-phase activity (Donahue et al., 2011b)), then condensation to the suspended particles will be quasi-irreversible. Furthermore, for the relatively low saturation concentration values required, there should be efficient wall losses of the vapors. We thus assume that vapor wall losses are the same per unit condensation sink as condensation to the suspended particles.

The condensation sink (*CS*) represents the loss frequency of vapors to the suspended aerosol surface (Donahue et al., 2014); it can be thought of as the mean speed of the vapors multiplied by the aerosol surface area, but modified for the gas-phase diffusion near the particle surface and accounting for accommodation from the gas phase to the condensed phase when that is rate limiting. We calculated the CS^P using equation 3 (Trump et al., 2014),

$$CS^P = \sum_k N_k \frac{v}{4} \pi d^2{}_{P,k} \beta_k \quad (3)$$

where *k* refers to a particle size bin, N_k is the number concentration of particles in this bin, v is the mean thermal speed of the gas phase molecules, $d_{P,k}$ is the particle diameter, and β_k is the transition-regime correction factor (Seinfeld and Pandis, 2006), which is a function of the mass accommodation coefficient (α) and the mean free path of the organic vapor in air. We used two accommodation coefficient values, 0.1 and 1, as limiting cases

Formatted: Justified

as the available evidence suggests that $0.1 < \alpha < 1$ (Saleh et al., 2013). When $\alpha = 1$, the condensation sink will be the same as the collision frequency between the gas molecules and suspended particles.

Fig. 5 shows the suspended collision frequency versus time together with the number and mass concentration of the suspended particles during an SOA formation experiment. The collision frequency decreased initially due to particle wall losses. However, when the SOA formation started, the SOA condensation increased the particle surface area and thus increased the collision frequency. Later in the experiment, after the SOA formation was almost complete, the particle wall loss again dominated and the collision frequency decreased.

As shown in Scheme 1, the fraction of the oxidation products that initially condenses on the suspended particles versus the chamber walls is determined by the ratio of the suspended-particle condensation sink to the wall loss frequency (the wall condensation sink). We previously measured a wall condensation sink for SVOCs in the CMU chamber of 0.063 min^{-1} (Ye et al., 2016a). In Fig. 6 we compare the suspended-particle condensation sink to the wall condensation sink for the two limiting values of the mass accommodation coefficient: 0.1 and 1. When $\alpha = 1$, the suspended-particle condensation sink is much larger than the wall condensation sink. In this case, only a very small fraction of the condensable vapors are lost to the walls, at least initially. When $\alpha = 0.1$, the condensation sink of the suspended particles and the chamber wall are comparable, which makes vapor wall loss significant.

The interactions of semi-volatile oxidation products with the two different sinks (suspended particles and the walls) can be complex, but products that are effectively nonvolatile (with very high steady-state saturation ratios while the PD is being oxidized (Donahue et al., 2011b)) should simply condense in proportion to the two condensation sinks. In this case the mass that condenses on the walls is given by the mass observed to condense on the suspended particles multiplied by the ratio of the wall condensation sink to the suspended condensation sink. In Fig. 7 we show the products lost to the chamber walls together with the SOA mass on the suspended particles and the particles lost to the chamber walls. The direct deposition of the product vapors to the chamber wall may have been as much as 1/3 of the total SOA mass at the lower limit of $\alpha = 0.1$ or as little as a few percent if $\alpha = 1$. This vapor wall loss correction is thus significant but not excessively large.

3.4 Correction for Delayed Condensation.

Some condensable products will be accumulated in the gas phase in a steady state between production and loss even if they have a very low saturation concentration. This is especially significant early in an experiment when the oxidation rate (and thus production rate of condensable vapors) is high (Donahue et al., 2011b). We can estimate this simply by assuming that the condensable vapors are produced with a constant mass yield during PD oxidation (that the mechanism is invariant) and that their saturation concentrations are very low. We then apply a constant mass fraction to the amount of oxidized PD to estimate the total concentration of condensable products in any phase. In Fig. 8, we show an example calculation for $\alpha = 0.1$ and a constant mass yield of 0.88 as a dashed black curve; except for early in the reaction, this provides a good match to the total condensed organics, but for times less than 2 condensation lifetimes (21 min, indicated with the vertical dashed red line)

the observed SOA concentration is substantially less than 0.88 times the oxidized PD (shown with the gray fill). The SOA mass yields during the first 10-20 minutes thus may be underestimated if delayed condensation is ignored (Donahue et al., 2011b). On the other hand, lower mass yields at lower OA concentrations can be interpreted in terms of semi-volatile partitioning (Odum et al., 1996b; Donahue et al., 2005).

3.5 ~~Overall~~ SOA mass yields from PD oxidation by OH radicals.

In Fig. 9 we show calculated SOA mass yields from the 6 ppb PD experiment for three cases, first considering only particle wall loss, and then treating both particle and vapor wall loss for $\alpha = 1$ and for $\alpha = 0.1$. When $\alpha = 1$, the difference with and without vapor wall losses (i.e. the first two cases) is very small. However, the mass yield increases by 30% after correcting for vapor wall loss with $\alpha = 0.1$. We further estimate the delayed condensation of ELVOC and LVOC products by finding the mass yield after two condensation lifetimes, as illustrated in Fig. 8. The dashed horizontal lines indicate these values. The true equilibrium SOA mass yields may be closer to the dashed lines than the observed values due to delayed condensation.

In Fig. 10 we summarize data from five experiments with five different initial PD concentrations: 1, 2, 4, 5, and 6 ppbv. The shaded area shows the range of SOA yields when α values vary from 0.1 to 1. The instantaneous SOA mass yields are from 0.1 to 0.9 under the different SOA concentrations. As with the single case we present in Fig 9, accounting for delayed condensation introduces a low-concentration asymptotic mass yield between 0.4 and 0.8. The bottom line is that regardless of the mass accommodation

coefficient the SOA mass yields are high, with yields above 0.5 for C_{OA} > 10 μg m^{-3}. PD oxidation by OH is thus a very efficient source of second-generation SOA.

The yields for α = 0.1 accounting for delayed condensation are implausibly high, implying that essentially all of the oxidation products have extremely low volatility and thus the only reason for the observed rising mass yields is the dynamical delay early in the experiment (which lasts for a relatively long time, ~20 min, due to the low condensation sink associated with the low mass accommodation coefficient). On the other hand, the yields for α = 1 are plausible, implying that approximately half of the condensable oxidation products consist of highly oxidized products formed via "auto oxidation" (Ehn et al., 2014) while the other half are SVOCs that partition reversibly into the particles (Ye et al., 2016b; Ye et al., 2016c).

PD oxidation has much higher SOA mass yields than α-pinene oxidation. When C_{OA} = 20 μg m^{-3}, the SOA mass yields from α-pinene oxidation (by ozone or OH) are in the range 0.1–0.2 (Hallquist et al., 2009), whereas the SOA mass yields from PD oxidation by OH are in the range 0.6–0.9, roughly five times larger. This finding holds regardless of wall effects or other complications to quantitative interpretation of the product volatility distribution, as those issues should be shared in common for each system. PD is a much more effective source of SOA than α-pinene. This can be well explained by the structure of PD. PD has two OH groups replacing the C=C double bond in α-pinene and yet it retains the bicyclic backbone of that monoterpene. PD can be considered as a first-generation of oxidation product of α-pinene; the likely atmospheric formation mechanism is hydrolysis of a β-hydroxy nitrate formed after OH addition to the double bond in high-NO_x conditions. When PD is oxidized, C-C bond cleavage is unlikely because of the bicyclic backbone. Therefore, most PD oxidation products will be less volatile than PD and so more

condensable compared to comparable products from α-pinene. One exception to this is that a major oxidation product of PD is oxy-pinocamphone, which is formed when OH abstracts a hydrogen atom from the hydroxymethylene moiety in PD and O_2 immediately abstracts the second hydrogen from the OH group, analogous to acetone formation from 2-propanol. All of the other oxidation products of PD are plausibly condensable. It is thus sensible that the molar yields of condensable products from PD oxidation are in the range 0.5–0.8 and that the corresponding mass yields are significantly higher due to the added oxygen.

3.6 Elemental analysis of the SOA.

In Fig. 11, we plot the observed average carbon oxidation state, $\overline{OS}_C = 2O:C - H:C$, of the SOA formed from PD as a function of the SOA mass concentration. $\overline{OS}_C$ decreases as the SOA mass increases, consistent with other studies of biogenic SOA (Donahue et al., 2006; Shilling et al., 2009). The SOA that condenses very early in the experiment (at low C_{OA}) is also highly oxidized. These promptly condensing organic products are ELVOCs or LVOCs, with sufficiently low volatility to build up a high saturation ratio early in the experiment. We also consistently observe a slight increase of $\overline{OS}_C$ at the end of each experiment. This may be due to the further oxidation (aging) of the products. The SOA formed from a lower initial PD concentration also shows a higher $\overline{OS}_C$ at the same SOA concentration than the SOA formed from a higher initial PD charge. When the initial PD concentration is low, the oxidation products may have more chance to react with OH radicals and become more oxidized. However, it is also possible that the higher absolute oxidation rate with higher PD concentrations drives up the gas-phase activity of SVOCs with relatively lower $\overline{OS}_C$. Finally, it is possible that relatively more volatile (and less oxidized) products are lost from SOA particles near the end of each experiment due to

sorption to the Teflon walls. As shown in Fig. S45, the ratio of organic to sulfate mass decreased slightly after 2 hours, consistent with some SOA mass loss from the particles.

The composition findings are thus consistent with the mass-yield results for a relatively high mass accommodation coefficient; there is a substantial mass yield of ELVOC and LVOC products with very high $\overline{OS}_C$ but also a significant yield of SVOC products, probably with $\overline{OS}_C \lesssim 1$, that dilute the (E)LVOC condensate once conditions favor their condensation.

In Fig. 11 we also compare the $\overline{OS}_C$ of the SOA formed from PD in these experiments with the $\overline{OS}_C$ of PD oxidation products observed to participate in nucleation in the CLOUD experiment. We plot values for CLOUD for molecular clusters with a single C_{10} molecule and clusters with 4 C_{10} molecules; these values are based on molecular formulas in negatively-charged clusters measured with an atmospheric pressure interface time of flight mass spectrometer (APITOF) where the negative charge resides on a bisulfate anion clustering with the (presumably neutral) C_{10} organic molecules formed from PD oxidation (Schobesberger et al., 2013). The CLOUD values are thus based on a much different technique than the highly fragmenting bulk particle electron ionization used in the AMS. Despite these differences, the $\overline{OS}_C$ values we observe are similar to those seen in the CLOUD experiments. The oxidized organics observed in the CLOUD experiments have molecular compositions $C_{10}H_xO_y$, where x = 12, 14, 16 and y = 2–12 (Schobesberger et al., 2013). They appear in four progressive bands from growing clusters, which contained 1-4 C_{10} organic molecules, respectively. The $\overline{OS}_C$ in the first band is relatively high, -0.2, but this decreases to -0.8 for the fourth band. The decrease of $\acute{O}S_C$ with increasing cluster size

is consistent with what we observed in this study. We observed the $\overline{OS}_C$ of the bulk SOA at relatively high loading was around -0.7, which corresponds to the value measured in the CLOUD experiments for larger clusters.

A self-consistent interpretation of these observations is that the least-volatile, early condensing species forming SOA at low C_{OA} in our experiments are ELVOCs that also help form the smallest clusters in the CLOUD experiments, while the later condensing species are LVOCs and SVOCs that also contribute to cluster growth in the CLOUD experiment after initial nucleation.

3.7 Representation of PD SOA in the two-dimensional volatility-oxidation space.

Following the procedures in the literature (Presto and Donahue, 2006; Donahue et al., 2011a), we mapped the distribution of volatility and $\overline{OS}_C$ in the two-dimensional volatility-oxidation space (2D-VBS). The constraints are relatively crude – just the observed mass concentrations and bulk composition, and so we present 2D-VBS yield distribution that is consistent with those constraints but still coarse grained. Specifically, we assume a long "tail" toward extremely low volatility with roughly constant mass yield, a cluster of products with slightly lower volatility than PD, and a large yield of oxy--pinocamphone, while is more volatile than PD. We present the full yield distribution, which conserves carbon, in the following section~~in the supplemental material~~.

In Fig. 12 we show the product distribution, classifying organics in the broad classes of ELVOCs, LVOCs, SVOCs or IVOCs when $\alpha = 1$. The top panel is a 2D representation. We show PD as a filled yellow circle. The blue contours show the oxidation products from PD, with higher values indicating higher yields. The lower panel is a consolidation of the

Formatted: Font: Not Bold

two-dimensional product contours into a 1D-VBS, showing the total mass yields in each decadally spaced volatility bin. A majority of the condensed products fall to the upper left of PD, with a lower volatility and higher $\overline{OS}_C$ than PD. These compounds are produced mostly by the addition of oxygen containing moieties to the PD backbone. However, some products located on the right of PD show slightly higher $\overline{OS}_C$, but also higher volatility. They may be formed by two possible reaction pathways. One is fragmentation, which breaks the carbon backbone and produces smaller molecules with higher volatility than the reactants. Another pathway is formation of oxy-pinocamphone, as discussed above.

The products at the end of the low-volatility tail extending toward the upper left in the top panel of Fig. 12 may contribute to the new-particle formation observed in the CLOUD experiments. These ELVOCs, with $\log C^o < -3.5$ are the most likely to form new particles because with constant mass yields the saturation ratio in each progressively less volatile bin will grow by an order of magnitude. The $\overline{OS}_C$ of these LVOC products ranges from 0 to 1, and they represent around 15 % of total SOA mass. This is consistent with CLOUD observations showing that ~10% of the PD oxidation products could drive new-particle formation (Schobesberger et al., 2013; Riccobono et al., 2014).

Employing the method of Chuang and Donahue (2016a), we conducted a dynamical simulation of SOA production following oxidation of 6 ppb PD in the CMU chamber, assuming a mass accommodation coefficient $\alpha = 1$. As shown in Fig. 13, the simulation describes the formation of condensable vapors and subsequent production of SOA mass. The suspended SOA mass in the simulation matches the smog-chamber data very well. The particle mass and SOA vapors lost to the Teflon chamber wall are also comparable with the calculated values from the experimental data. Especially during the first 15 minutes,

574 the simulation shows there is a large fraction of condensable SOA vapors in the gas phase.
575 This agrees with the observed condensation delay due to the condensation sink timescale.

576 **4 Conclusions**

577 Our studies show that oxidation of pinanediol, a semi-volatile surrogate for first-generation
578 oxidation products of monoterpenes, can produce SOA with very high mass yields. The
579 SOA is also highly oxidized. This is thus a model system to describe chemical aging of
580 first-generation SOA. Along with previously studied model systems for first-generation
581 products, this shows that aging of semi-volatile SOA is a significant source of additional
582 SOA mass, with higher mass yields typical of less volatile first-generation products. The
583 second-generation oxidation products with sufficiently low volatility represent 15% of the
584 total SOA mass in a 2D-VBS model that reproduces the chamber data; these may contribute
585 to new-particle formation. The oxidation state of the chamber SOA produced from
586 oxidation of PD is also consistent with the observations during new-particle formation
587 experiments at CERN. Thus, while first-generation oxidation is a substantial source of both
588 SOA mass and new-particle formation, ongoing oxidation of first-generation vapors, which
589 typically comprise the large majority of the first-generation oxidation products from
590 common precursors, should also be considered as a significant source of both particle
591 number and mass.

592 *Competing interests.* The authors declare that they have no conflict of interest.

593 *Acknowledgments.* This research was supported by grant AGS1136479 and AGS1447056,
594 from the National Science Foundation. The High-Resolution Aerosol Mass Spectrometer

595 was purchased with Major Research Instrumentation funds from NSF CBET0922643 and
596 the Wallace Research Foundation.

References

Chacon-Madrid, H. J., Presto, A. A., and Donahue, N. M.: Functionalization vs. fragmentation: n-aldehyde oxidation mechanisms and secondary organic aerosol formation, Physical Chemistry Chemical Physics, 12, 13975-13982, 10.1039/C0CP00200C, 2010.

Chacon-Madrid, H. J., and Donahue, N. M.: Fragmentation vs. functionalization: chemical aging and organic aerosol formation, Atmospheric Chemistry and Physics, 11, 10553-10563, 10.5194/acp-11-10553-2011, 2011.

Chacon-Madrid, H. J., Murphy, B. N., Pandis, S. N., and Donahue, N. M.: Simulations of smog-chamber experiments using the two-dimensional volatility basis set: linear oxygenated precursors, Environmental Science & Technology, 46, 11179-11186, 10.1021/es3017232, 2012.

Chacon-Madrid, H. J., Henry, K. M., and Donahue, N. M.: Photo-oxidation of pinonaldehyde at low NO_x: from chemistry to organic aerosol formation, Atmospheric Chemistry and Physics, 13, 3227-3236, 10.5194/acp-13-3227-2013, 2013.

Chuang, W. K., and Donahue, N. M.: Dynamic Consideration of Smog Chamber Experiments, Atmospheric Chemistry and Physics, 17, 10019-10036, 10.5194/acp-17-10019-2017, 2017.

Chuang, W. K., and Donahue, N. M.: A two-dimensional volatility basis set – Part 3: Prognostic modeling and NOx dependence, Atmospheric Chemistry and Physics, 16, 123-134,10.5194/acp-16-123-2016, 2016b.

Cubison, M. J., Ortega, A. M., Hayes, P. L., Farmer, D. K., Day, D., Lechner, M. J., Brune, W. H., Apel, E., Diskin, G. S., Fisher, J. A., Fuelberg, H. E., Hecobian, A., Knapp, D. J., Mikoviny, T., Riemer, D., Sachse, G. W., Sessions, W., Weber, R. J., Weinheimer, A. J., Wisthaler, A., and Jimenez, J. L.: Effects of aging on organic aerosol from open biomass burning smoke in aircraft and laboratory studies, Atmospheric Chemistry and Physics, 11, 12049-12064, 10.5194/acp-11-12049-2011, 2011.

Donahue, N., Robinson, A., Trump, E., Riipinen, I., and Kroll, J.: Volatility and Aging of Atmospheric Organic Aerosol, in: Atmospheric and Aerosol Chemistry, edited by: McNeill, V. F., and Ariya, P. A., Topics in Current Chemistry, Springer Berlin Heidelberg, 97-143, 2014.

Donahue, N. M., Huff Hartz, K. E., Chuong, B., Presto, A. A., Stanier, C. O., Rosenhorn, T., Robinson, A. L., and Pandis, S. N.: Critical factors determining the variation in SOA yields from terpene ozonolysis: A combined experimental and computational study, Faraday Discussions, 130, 295-309, 10.1039/B417369D, 2005.

Donahue, N. M., Robinson, A. L., Stanier, C. O., and Pandis, S. N.: Coupled Partitioning, Dilution, and Chemical Aging of Semivolatile Organics, Environmental Science & Technology, 40, 2635-2643, 10.1021/es052297c, 2006.

Donahue, N. M., Epstein, S. A., Pandis, S. N., and Robinson, A. L.: A two-dimensional volatility basis set: 1. organic-aerosol mixing thermodynamics, Atmospheric Chemistry and Physics, 11, 3303-3318, 10.5194/acp-11-3303-2011, 2011a.

Donahue, N. M., Trump, E. R., Pierce, J. R., and Riipinen, I.: Theoretical constraints on pure vapor-pressure driven condensation of organics to ultrafine particles, Geophysical Research Letters, 38, L16801, 10.1029/2011GL048115, 2011b.

Donahue, N. M., Trump, E. R., Pierce, J. R., and Riipinen, I.: Theoretical constraints on pure vapor-pressure driven condensation of organics to ultrafine particles, Geophysical Research Letters, 38, L16801, 10.1029/2011GL048115, 2011c.

Donahue, N. M., Henry, K. M., Mentel, T. F., Kiendler-Scharr, A., Spindler, C., Bohn, B., Brauers, T., Dorn, H. P., Fuchs, H., Tillmann, R., Wahner, A., Saathoff, H., Naumann, K.-H., Möhler, O., Leisner, T., Müller, L., Reinnig, M.-C., Hoffmann, T., Salo, K., Hallquist, M., Frosch, M., Bilde, M., Tritscher, T., Barmet, P., Praplan, A. P., DeCarlo, P. F., Dommen, J., Prévôt, A. S. H., and Baltensperger, U.: Aging of biogenic secondary organic aerosol via gas-phase OH radical reactions, Proceedings of the National Academy of Sciences, 109, 13503-13508, 10.1073/pnas.1115186109, 2012a.

Donahue, N. M., Kroll, J. H., Pandis, S. N., and Robinson, A. L.: A two-dimensional volatility basis set – Part 2: Diagnostics of organic-aerosol evolution, Atmospheric Chemistry and Physics, 12, 615-634, 10.5194/acp-12-615-2012, 2012b.

Donahue, N. M., Chuang, W., Epstein, S. A., Kroll, J. H., Worsnop, D. R., Robinson, A. L., Adams, P. J., and Pandis, S. N.: Why do organic aerosols exist? Understanding aerosol lifetimes using the two-dimensional volatility basis set, Environmental Chemistry, 10, 151-157, 2013.

Duplissy, J., Merikanto, J., Franchin, A., Tsagkogeorgas, G., Kangasluoma, J., Wimmer, D., Vuollekoski, H., Schobesberger, S., Lehtipalo, K., Flagan, R. C., Brus, D., Donahue, N. M., Vehkamäki, H., Almeida, J., Amorim, A., Barmet, P., Bianchi, F., Breitenlechner, M., Dunne, E. M., Guida, R., Henschel, H., Junninen, H., Kirkby, J., Kürten, A., Kupc, A., Määttänen, A., Makhmutov, V., Mathot, S., Nieminen, T., Onnela, A., Praplan, A. P., Riccobono, F., Rondo, L., Steiner, G., Tome, A., Walther, H., Baltensperger, U., Carslaw, K. S., Dommen, J., Hansel, A., Petäjä, T., Sipilä, M., Stratmann, F., Vrtala, A., Wagner, P. E., Worsnop, D. R., Curtius, J., and Kulmala, M.: Effect of ions on sulfuric acid-water binary particle formation: 2. Experimental data and comparison with QC-normalized classical nucleation theory, Journal of Geophysical Research: Atmospheres, 121, 1752-1775, 10.1002/2015JD023539, 2016.

Ehn, M., Thornton, J. A., Kleist, E., Sipila, M., Junninen, H., Pullinen, I., Springer, M., Rubach, F., Tillmann, R., Lee, B., Lopez-Hilfiker, F., Andres, S., Acir, I.-H., Rissanen, M., Jokinen, T., Schobesberger, S., Kangasluoma, J., Kontkanen, J., Nieminen, T., Kurten, T., Nielsen, L. B., Jorgensen, S., Kjaergaard, H. G., Canagaratna, M., Maso, M. D., Berndt, T., Petaja, T., Wahner, A., Kerminen, V.-M., Kulmala, M., Worsnop, D. R., Wildt, J., and Mentel, T. F.: A large source of low-volatility secondary organic aerosol, Nature, 506, 476-479, 10.1038/nature13032, 2014.

Hallquist, M., Wenger, J. C., Baltensperger, U., Rudich, Y., Simpson, D., Claeys, M., Dommen, J., Donahue, N. M., George, C., Goldstein, A. H., Hamilton, J. F., Herrmann, H., Hoffmann, T., Iinuma, Y., Jang, M., Jenkin, M. E., Jimenez, J. L., Kiendler-Scharr, A., Maenhaut, W., McFiggans, G., Mentel, T. F., Monod, A., Prévôt, A. S. H., Seinfeld, J. H., Surratt, J. D., Szmigielski, R., and Wildt, J.: The formation, properties and impact of secondary organic aerosol: current and emerging issues, Atmospheric Chemistry and Physics, 9, 5155-5236, 10.5194/acp-9-5155-2009, 2009.

Henry, K. M., and Donahue, N. M.: Photochemical aging of α-pinene secondary organic aerosol: Effects of OH radical sources and photolysis, The Journal of Physical Chemistry A, 116, 5932-5940, 10.1021/jp210288s, 2012.

Hildebrandt, L., Donahue, N. M., and Pandis, S. N.: High formation of secondary organic aerosol from the photo-oxidation of toluene, Atmospheric Chemistry and Physics, 9, 2973-2986, 2009.

Jang, M., and Kamens, R. M.: Newly characterized products and composition of secondary aerosols from the reaction of α-pinene with ozone, Atmospheric Environment, 33, 459-474, 1999.

Jaoui, M., and Kamens, R. M.: Mass balance of gaseous and particulate products analysis from α-pinene/NO x /air in the presence of natural sunlight, Journal of Geophysical Research: Atmospheres, 106, 12541-12558, 10.1029/2001JD900005, 2001.

Kanakidou, M., Seinfeld, J. H., Pandis, S. N., Barnes, I., Dentener, F. J., Facchini, M. C., Dingenen, R. V., Ervens, B., Nenes, A., Nielsen, C. J., Swietlicki, E., Putaud, J. P., Balkanski, Y., Fuzzi, S., Horth, J., Moortgat, G. K., Winterhalter, R., Myhre, C. E. L., Tsigaridis, K., Vignati, E., Stephanou, E. G., and Wilson, J.: Organic aerosol and global climate modelling: a review, Atmospheric Chemistry and Physics, 5, 1053-1123, 2005.

Kirkby, J., Curtius, J., Almeida, J., Dunne, E., Duplissy, J., Ehrhart, S., Franchin, A., Gagne, S., Ickes, L., Kurten, A., Kupc, A., Metzger, A., Riccobono, F., Rondo, L., Schobesberger, S., Tsagkogeorgas, G., Wimmer, D., Amorim, A., Bianchi, F., Breitenlechner, M., David, A., Dommen, J., Downard, A., Ehn, M., Flagan, R. C., Haider, S., Hansel, A., Hauser, D., Jud, W., Junninen, H., Kreissl, F., Kvashin, A., Laaksonen, A., Lehtipalo, K., Lima, J., Lovejoy, E. R., Makhmutov, V., Mathot, S., Mikkila, J., Minginette, P., Mogo, S., Nieminen, T., Onnela, A., Pereira, P., Petaja, T., Schnitzhofer, R., Seinfeld, J. H., Sipila, M., Stozhkov, Y., Stratmann, F.,

Tome, A., Vanhanen, J., Viisanen, Y., Vrtala, A., Wagner, P. E., Walther, H., Weingartner, E., Wex, H., Winkler, P. M., Carslaw, K. S., Worsnop, D. R., Baltensperger, U., and Kulmala, M.: Role of sulphuric acid, ammonia and galactic cosmic rays in atmospheric aerosol nucleation, Nature, 476, 429-433, 2011.

Krechmer, J. E., Pagonis, D., Ziemann, P. J., and Jimenez, J. L.: Quantification of Gas-Wall Partitioning in Teflon Environmental Chambers Using Rapid Bursts of Low-Volatility Oxidized Species Generated in Situ, Environmental Science & Technology, 50, 5757-5765, 10.1021/acs.est.6b00606, 2016.

Kroll, J. H., Smith, J. D., Che, D. L., Kessler, S. H., Worsnop, D. R., and Wilson, K. R.: Measurement of fragmentation and functionalization pathways in the heterogeneous oxidation of oxidized organic aerosol, Physical Chemistry Chemical Physics, 11, 8005-8014, 10.1039/B905289E, 2009.

Lambe, A. T., Ahern, A. T., Williams, L. R., Slowik, J. G., Wong, J. P. S., Abbatt, J. P. D., Brune, W. H., Ng, N. L., Wright, J. P., Croasdale, D. R., Worsnop, D. R., Davidovits, P., and Onasch, T. B.: Characterization of aerosol photooxidation flow reactors: heterogeneous oxidation, secondary organic aerosol formation and cloud condensation nuclei activity measurements, Atmospheric Measurement Techniques, 4, 445-461, 10.5194/amt-4-445-2011, 2011.

Matsunaga, A., and Ziemann ‡, P. J.: Gas-Wall Partitioning of Organic Compounds in a Teflon Film Chamber and Potential Effects on Reaction Product and Aerosol Yield Measurements, Aerosol Science and Technology, 44, 881-892, 10.1080/02786826.2010.501044, 2010.

May, A. A., Saleh, R., Hennigan, C. J., Donahue, N. M., and Robinson, A. L.: Volatility of Organic Molecular Markers Used for Source Apportionment Analysis: Measurements and Implications for Atmospheric Lifetime, Environmental Science & Technology, 46, 12435-12444, 10.1021/es302276t, 2012.

Müller, L., Reinnig, M. C., Naumann, K. H., Saathoff, H., Mentel, T. F., Donahue, N. M., and Hoffmann, T.: Formation of 3-methyl-1,2,3-butanetricarboxylic acid via gas phase oxidation of pinonic acid – a mass spectrometric study of SOA aging, Atmospheric Chemistry and Physics, 12, 1483-1496, 10.5194/acp-12-1483-2012, 2012.

Nakao, S., Tang, P., Tang, X., Clark, C. H., Qi, L., Seo, E., Asa-Awuku, A., and Cocker Iii, D.: Density and elemental ratios of secondary organic aerosol: Application of a density prediction method, Atmospheric Environment, 68, 273-277, 2013.

Odum, J. R., Hoffmann, T., Bowman, F., Collins, D., Flagan, R. C., and Seinfeld, J. H.: Gas/particle partitioning and secondary organic aerosol yields, Environmental Science & Technology, 30, 2580-2585, 1996a.

Odum, J. R., Hoffmann, T., Bowman, F., Collins, D., Flagan, R. C., and Seinfeld, J. H.: Gas/Particle Partitioning and Secondary Organic Aerosol Yields, Environmental Science & Technology, 30, 2580-2585, 10.1021/es950943+, 1996b.

Pandis, S. N., Paulson, S. E., Seinfeld, J. H., and Flagan, R. C.: Aerosol formation in the photooxidation of isoprene and β-pinene, Atmospheric Environment, 25A, 997-1008, 1991.

Pope, C. A., Ezzati, M., and Dockery, D. W.: Fine-Particulate Air Pollution and Life Expectancy in the United States, New England Journal of Medicine, 360, 376-386, doi:10.1056/NEJMsa0805646, 2009.

Presto, A. A., and Donahue, N. M.: Investigation of α-Pinene + Ozone Secondary Organic Aerosol Formation at Low Total Aerosol Mass, Environmental Science & Technology, 40, 3536-3543, 10.1021/es052203z, 2006.

Qi, L., Nakao, S., and Cocker, D. R.: Aging of secondary organic aerosol from α-pinene ozonolysis: Roles of hydroxyl and nitrate radicals, Journal of the Air & Waste Management Association, 62, 1359-1369, 10.1080/10962247.2012.712082, 2012.

Riccobono, F., Schobesberger, S., Scott, C. E., Dommen, J., Ortega, I. K., Rondo, L., Almeida, J., Amorim, A., Bianchi, F., Breitenlechner, M., David, A., Downard, A., Dunne, E. M., Duplissy, J., Ehrhart, S., Flagan, R. C., Franchin, A., Hansel, A., Junninen, H., Kajos, M., Keskinen, H.,

Kupc, A., Kürten, A., Kvashin, A. N., Laaksonen, A., Lehtipalo, K., Makhmutov, V., Mathot, S., Nieminen, T., Onnela, A., Petäjä, T., Praplan, A. P., Santos, F. D., Schallhart, S., Seinfeld, J. H., Sipilä, M., Spracklen, D. V., Stozhkov, Y., Stratmann, F., Tomé, A., Tsagkogeorgas, G., Vaattovaara, P., Viisanen, Y., Vrtala, A., Wagner, P. E., Weingartner, E., Wex, H., Wimmer, D., Carslaw, K. S., Curtius, J., Donahue, N. M., Kirkby, J., Kulmala, M., Worsnop, D. R., and Baltensperger, U.: Oxidation Products of Biogenic Emissions Contribute to Nucleation of Atmospheric Particles, Science, 344, 717-721, 10.1126/science.1243527, 2014.

Robinson, E. S., Saleh, R., and Donahue, N. M.: Organic aerosol mixing observed by single-particle mass spectrometry, The Journal of Physical Chemistry A, 117,13935-13945, 10.1021/jp405789t, 2013.

Saleh, R., Donahue, N. M., and Robinson, A. L.: Time Scales for Gas-Particle Partitioning Equilibration of Secondary Organic Aerosol Formed from Alpha-Pinene Ozonolysis, Environmental Science & Technology, 47, 5588-5594, 10.1021/es400078d, 2013.

Schobesberger, S., Junninen, H., Bianchi, F., Lönn, G., Ehn, M., Lehtipalo, K., Dommen, J., Ehrhart, S., Ortega, I. K., Franchin, A., Nieminen, T., Riccobono, F., Hutterli, M., Duplissy, J., Almeida, J., Amorim, A., Breitenlechner, M., Downard, A. J., Dunne, E. M., Flagan, R. C., Kajos, M., Keskinen, H., Kirkby, J., Kupc, A., Kürten, A., Kurtén, T., Laaksonen, A., Mathot, S., Onnela, A., Praplan, A. P., Rondo, L., Santos, F. D., Schallhart, S., Schnitzhofer, R., Sipilä, M., Tomé, A., Tsagkogeorgas, G., Vehkamäki, H., Wimmer, D., Baltensperger, U., Carslaw, K. S., Curtius, J., Hansel, A., Petäjä, T., Kulmala, M., Donahue, N. M., and Worsnop, D. R.: Molecular understanding of atmospheric particle formation from sulfuric acid and large oxidized organic molecules, Proceedings of the National Academy of Sciences, 110, 17223-17228, 10.1073/pnas.1306973110, 2013.

Seinfeld, J. H., and Pandis, S. N.: Atmospheric chemistry and physics — from air pollution to climate change, 2nd ed., John Wiley & Sons, New York, 2006.

Shilling, J. E., Chen, Q., King, S. M., Rosenoern, T., Kroll, J. H., Worsnop, D. R., DeCarlo, P. F., Aiken, A. C., Sueper, D., Jimenez, J. L., and Martin, S. T.: Loading-dependent elemental composition of α-pinene SOA particles, Atmospheric Chemistry and Physics, 9, 771-782, 10.5194/acp-9-771-2009, 2009.

Solomon, S. Q., D.; Manning, M.; Alley, R. B.; Berntsen, T.; Bindoff, N. L.; Chen, Z.; Chidthaisong, A.; Gregory, J. M.; Hegerl, G. C.: Climate change 2007: The physical science basis, contribution of working group 1 to the fourth assessment report of the Intergovernmental Panel on Climate Change, 2007.

Tkacik, D. S., Lambe, A. T., Jathar, S., Li, X., Presto, A. A., Zhao, Y., Blake, D., Meinardi, S., Jayne, J. T., Croteau, P. L., and Robinson, A. L.: Secondary Organic Aerosol Formation from in-Use Motor Vehicle Emissions Using a Potential Aerosol Mass Reactor, Environmental Science & Technology, 48, 11235-11242, 10.1021/es502239v, 2014.

Tröstl, J., Chuang, W. K., Gordon, H., Heinritzi, M., Yan, C., Molteni, U., Ahlm, L., Frege, C., Bianchi, F., Wagner, R., Simon, M., Lehtipalo, K., Williamson, C., Craven, J. S., Duplissy, J., Adamov, A., Almeida, J., Bernhammer, A.-K., Breitenlechner, M., Brilke, S., Dias, A., Ehrhart, S., Flagan, R. C., Franchin, A., Fuchs, C., Guida, R., Gysel, M., Hansel, A., Hoyle, C. R., Jokinen, T., Junninen, H., Kangasluoma, J., Keskinen, H., Kim, J., Krapf, M., Kürten, A., Laaksonen, A., Lawler, M., Leiminger, M., Mathot, S., Möhler, O., Nieminen, T., Onnela, A., Petäjä, T., Piel, F. M., Miettinen, P., Rissanen, M. P., Rondo, L., Sarnela, N., Schobesberger, S., Sengupta, K., Sipilä, M., Smith, J. N., Steiner, G., Tomè, A., Virtanen, A., Wagner, A. C., Weingartner, E., Wimmer, D., Winkler, P. M., Ye, P., Carslaw, K. S., Curtius, J., Dommen, J., Kirkby, J., Kulmala, M., Riipinen, I., Worsnop, D. R., Donahue, N. M., and Baltensperger, U.: The role of low-volatility organic compounds in initial particle growth in the atmosphere, Nature, 533, 527-531, 10.1038/nature18271, 2016.

Trump, E. R., Riipinen, I., and Donahue, N. M.: Interactions between atmospheric ultrafine particles and secondary organic aerosol mass: a model study, Boreal Environment Research, 19, 352–362, 2014.

Trump, E. R., Epstein, S. A., Riipinen, I., and Donahue, N. M.: Wall effects in smog chamber experiments: A model study, Aerosol Science and Technology, 50, 1180-1200, 10.1080/02786826.2016.1232858, 2016.

Wong, J. P. S., Lee, A. K. Y., Slowik, J. G., Cziczo, D. J., Leaitch, W. R., Macdonald, A., and Abbatt, J. P. D.: Oxidation of ambient biogenic secondary organic aerosol by hydroxyl radicals: Effects on cloud condensation nuclei activity, Geophysical Research Letters, 38, L22805, 10.1029/2011GL049351, 2011.

Ye, P., Ding, X., Hakala, J., Hofbauer, V., Robinson, E. S., and Donahue, N. M.: Vapor wall loss of semi-volatile organic compounds in a Teflon chamber, Aerosol Science and Technology, 50, 822-834, 10.1080/02786826.2016.1195905, 2016a.

Ye, P., Ding, X., Ye, Q., Robinson, E. S., and Donahue, N. M.: Uptake of Semivolatile Secondary Organic Aerosol Formed from α-Pinene into Nonvolatile Polyethylene Glycol Probe Particles, The Journal of Physical Chemistry A, 120, 1459-1467, 10.1021/acs.jpca.5b07435, 2016b.

Ye, Q., Robinson, E. S., Ding, X., Ye, P., Sullivan, R. C., and Donahue, N. M.: Mixing of secondary organic aerosols versus relative humidity, Proceedings of the National Academy of Sciences, 113, 12649-12654, 10.1073/pnas.1604536113, 2016c.

Zhang, Q., Jimenez, J. L., Canagaratna, M. R., Allan, J. D., Coe, H., Ulbrich, I., Alfarra, M. R., Takami, A., Middlebrook, A. M., Sun, Y. L., Dzepina, K., Dunlea, E., Docherty, K., DeCarlo, P. F., Salcedo, D., Onasch, T., Jayne, J. T., Miyoshi, T., Shimono, A., Hatakeyama, S., Takegawa, N., Kondo, Y., Schneider, J., Drewnick, F., Borrmann, S., Weimer, S., Demerjian, K., Williams, P., Bower, K., Bahreini, R., Cottrell, L., Griffin, R. J., Rautiainen, J., Sun, J. Y., Zhang, Y. M., and Worsnop, D. R.: Ubiquity and dominance of oxygenated species in organic aerosols in anthropogenically-influenced Northern Hemisphere midlatitudes, Geophysical Research Letters, 34, L13801, 10.1029/2007GL029979, 2007.

Zhang, X., McVay, R. C., Huang, D. D., Dalleska, N. F., Aumont, B., Flagan, R. C., and Seinfeld, J. H.: Formation and evolution of molecular products in α-pinene secondary organic aerosol, Proceedings of the National Academy of Sciences, 112, 14168-14173, 10.1073/pnas.1517742112, 2015a.

Zhang, X., Schwantes, R. H., McVay, R. C., Lignell, H., Coggon, M. M., Flagan, R. C., and Seinfeld, J. H.: Vapor wall deposition in Teflon chambers, Atmos. Chem. Phys., 15, 4197-4214, 10.5194/acp-15-4197-2015, 2015b.

Zhao, Y., Hennigan, C. J., May, A. A., Tkacik, D. S., de Gouw, J. A., Gilman, J. B., Kuster, W. C., Borbon, A., and Robinson, A. L.: Intermediate-Volatility Organic Compounds: A Large Source of Secondary Organic Aerosol, Environmental Science & Technology, 48, 13743-13750, 10.1021/es5035188, 2014.

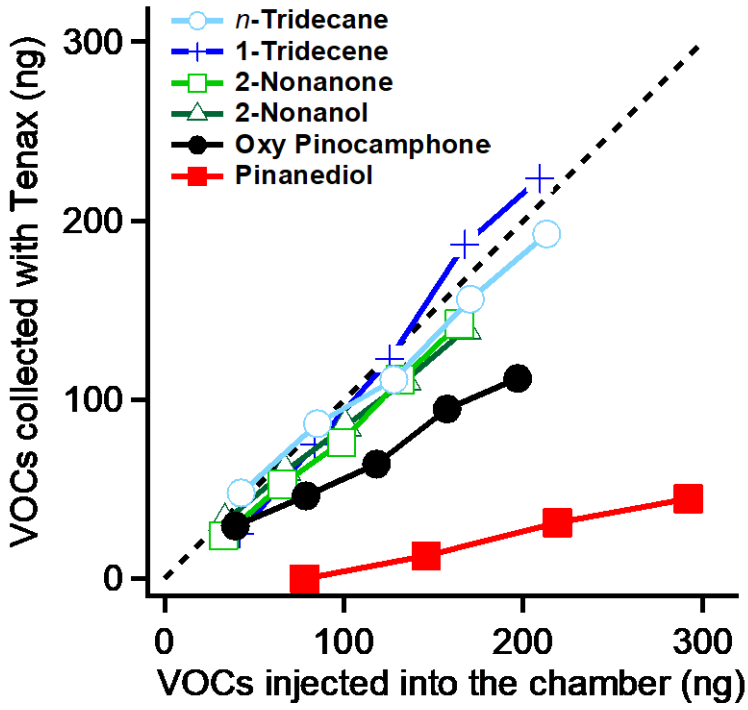

836

837 **Figure 1.** The gas phase concentrations of *n*-tridecane, 1-tridecene, 2-nonanone, 2-Nonanol, oxy-
838 pinocamphone and pinanediol in the chamber measured by TDGC/MS. Compared to the amount of organics
839 injected into the chamber, *n*-tridecane, 1-tridecene, 2-nonanone and 2-nonanol show almost no vapor wall
840 loss. Oxy-pinocamphone and pinanediol show 43% and 86% loss, respectively.

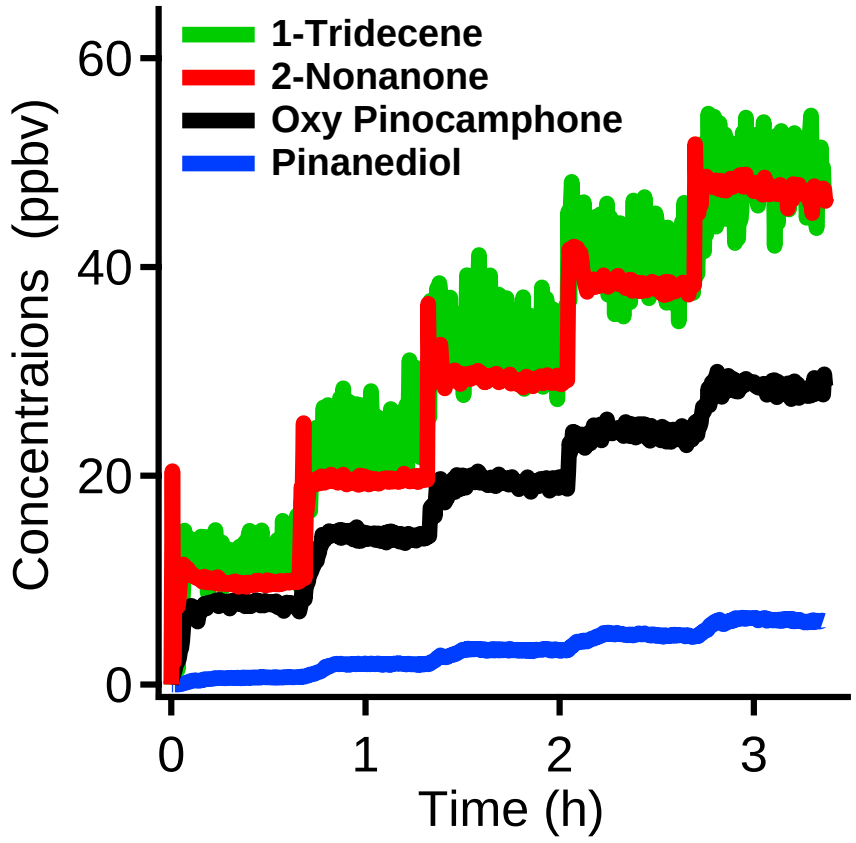

841

842 **Figure 2.** The temporal concentrations of the organics after we injected a series of aliquots of 1-tridencene,
843 2-nonanone, oxy-pinocamphone and pinanediol into the chamber in increments of 11 ppbv (at 100%
844 injection efficiency). Each injection resulted in a similar increase of all organics. The similar increase
845 indicates that oxy-pinocamphone and pinanediol may have constant wall loss factors in the concentration
846 range studied in this work.

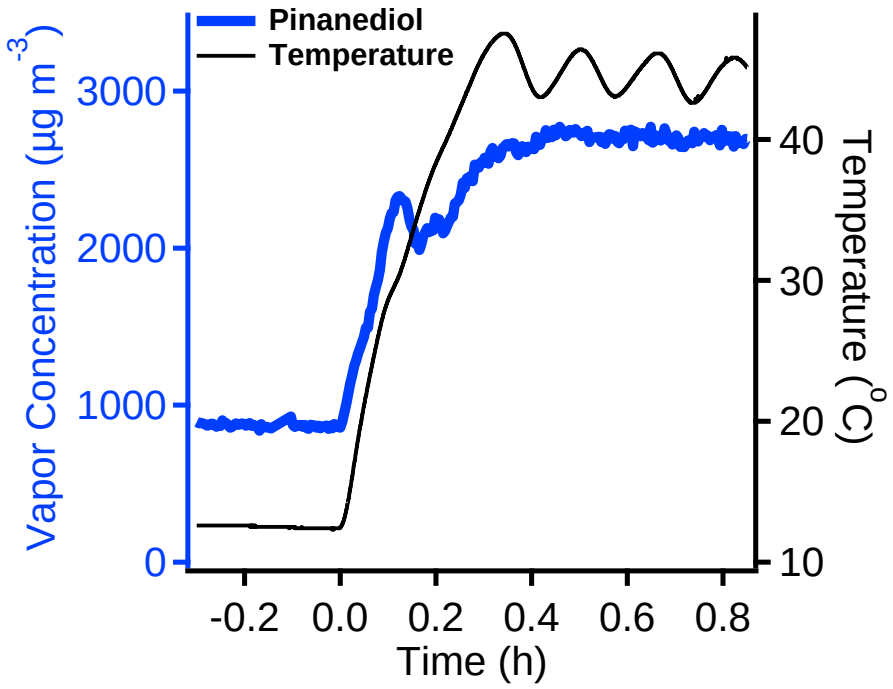

847

848 **Figure 3.** The increase of the pinanediol vapor concentration after increasing the chamber temperature from
849 13 °C to 44 °C. The concentration of PD increased 2.5-3 times and reached a constant value after temperature
850 stabilized at 44 °C. The increase of the PD concentration shows that PD can come out from the chamber walls
851 at higher temperature.

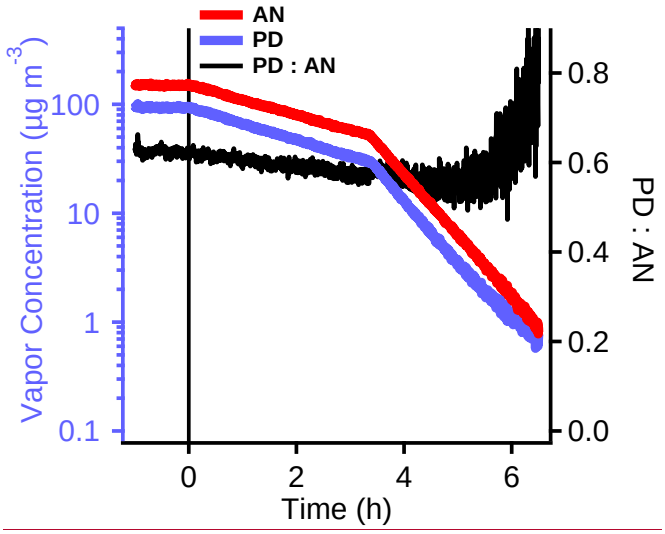

852

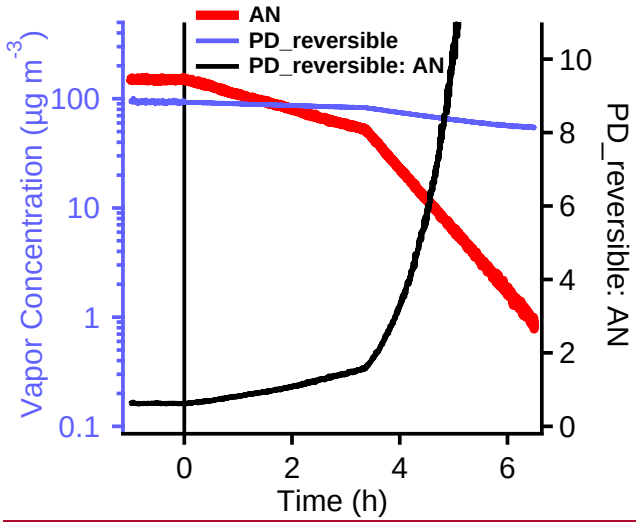

853

Formatted: Justified

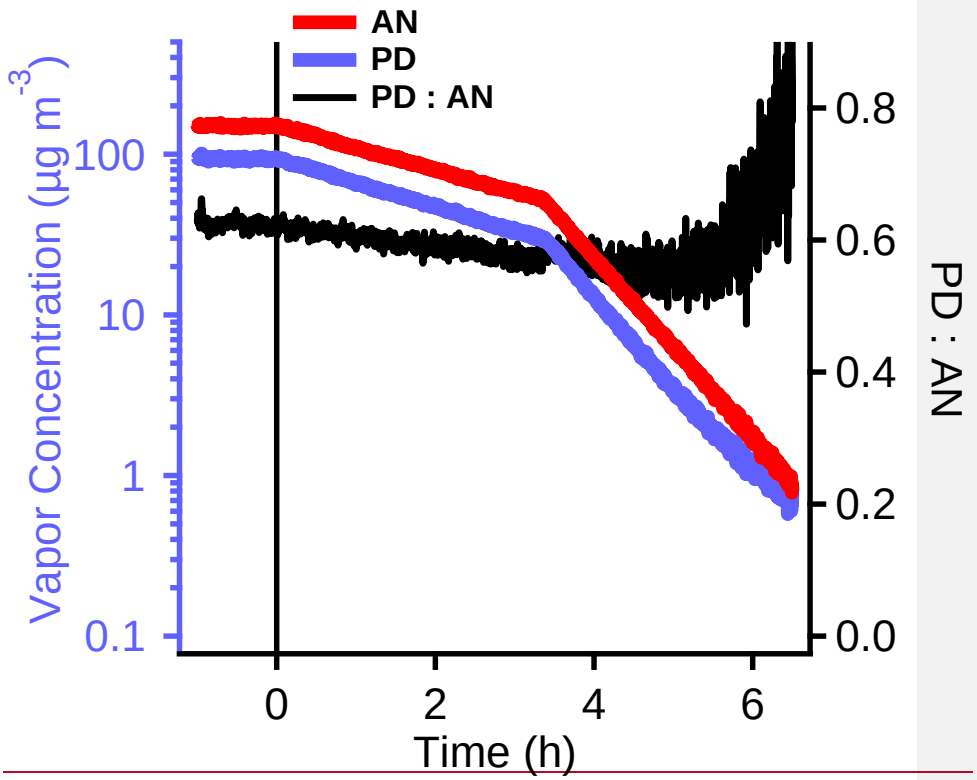

Figure 4. The change of PD and AN concentrations during isothermal dilution of the chamber with fresh air, which mimics the depletion of PD during the SOA formation (Top). The ratio of PD to AN shows very small change until the PD concentration dropped below 2 µg m^{-3}. When considering the deposition of PD on the Teflon chamber walls as reversible partitioning, the predicted PD and AN concentration change during the dilution was shown at the bottom. The decrease of the predicted PD concentration should be slower than the decrease of AN. The ratio of the predicted PD to AN concentration should keep increasing. These~~is~~ indicate~~s~~ that PD does not return to the gas phase from the Teflon at 22 °C, but instead still shows a modest loss to the chamber walls. So no further correction for the release or loss of PD is necessary when studying the SOA formation.

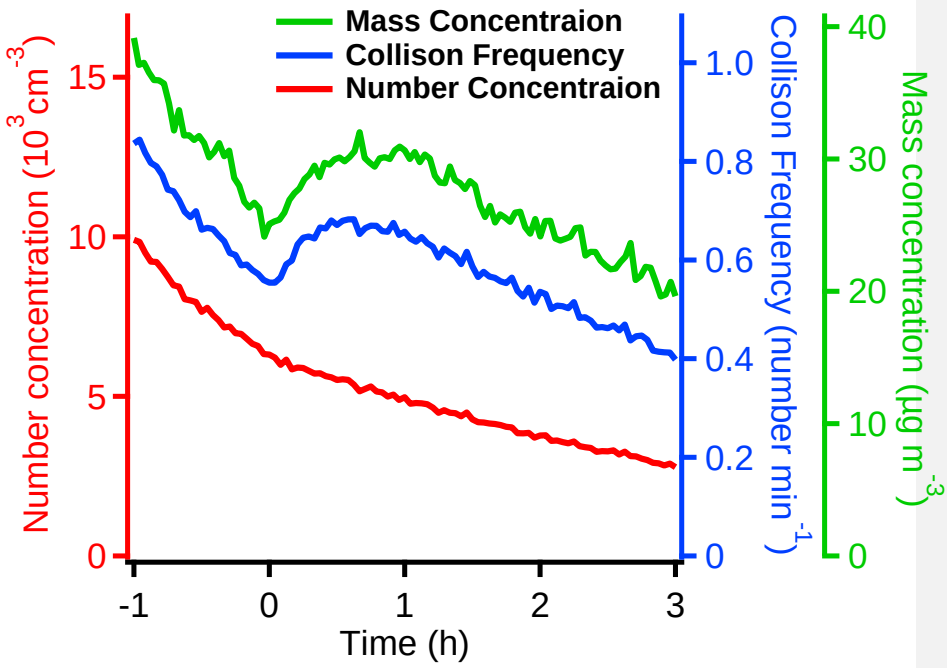

Figure 5. The change of collision frequency and number, mass concentration of the suspended particles during the SOA formation. The collision frequency has the same value as condensation sink when α=1. After the SOA formation started at 0h, the SOA mass condensed on the particles increased the particle surface areas and increased the collision frequency. We also observed the increase of the total mass concentrations. The particle number concentration always followed the exponential decay which indicated the nucleation may be minimal.

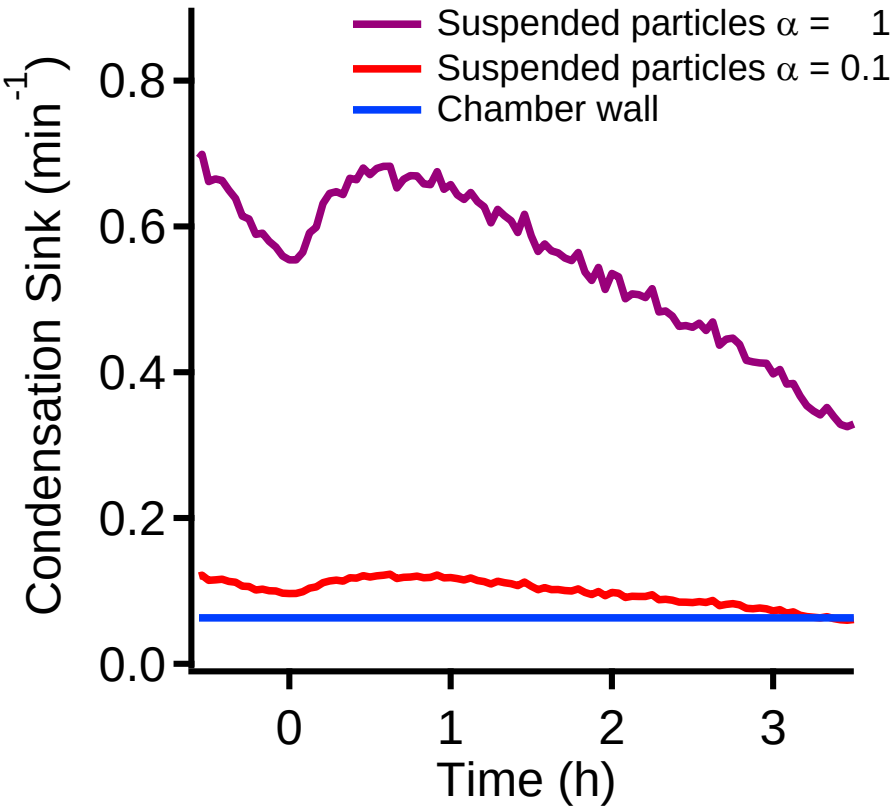

871

872 **Figure 6.** The difference of the condensation sink between the chamber wall with the suspended particles
873 when the mass accommodation coefficient is 0.1 or 1. When α = 1, the condensaiton sink of the suspended
874 particles is much larger than the wall condensation sink. When α = 0.1, the two values are on a similar level
875 which indicates that the vapor wall loss may be very significant.

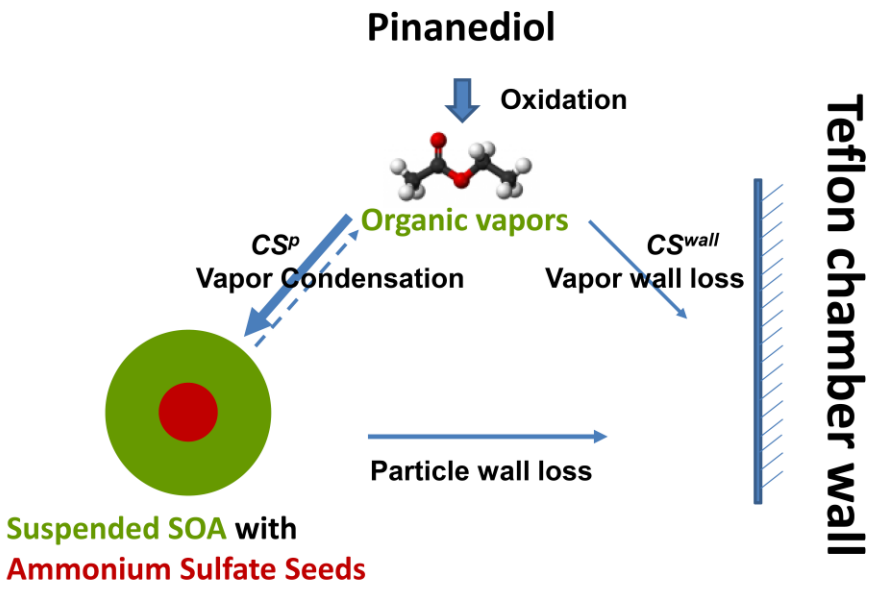

876

877 **Scheme 1.** The competition of vapor deposition on the suspended particles and the Teflon chamber walls.
878 The fraction of the oxidation products deposited on the suspended particles and the chamber wall are
879 determined by the condensation sink to the particles and the chamber walls

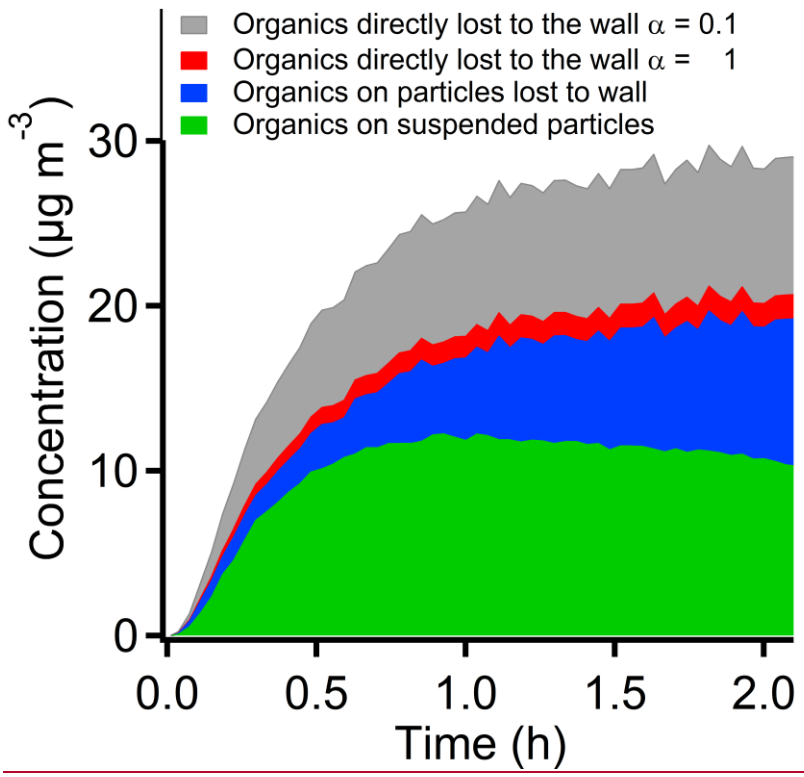
Organics directly lost to the wall α = 0.1
Organics directly lost to the wall α = 1
Organics on particles lost to wall
Organics on suspended particles
Concentration (μg m-3)
0
10
20
30
0.0
0.5
1.0
1.5
2.0
Time (h)

880

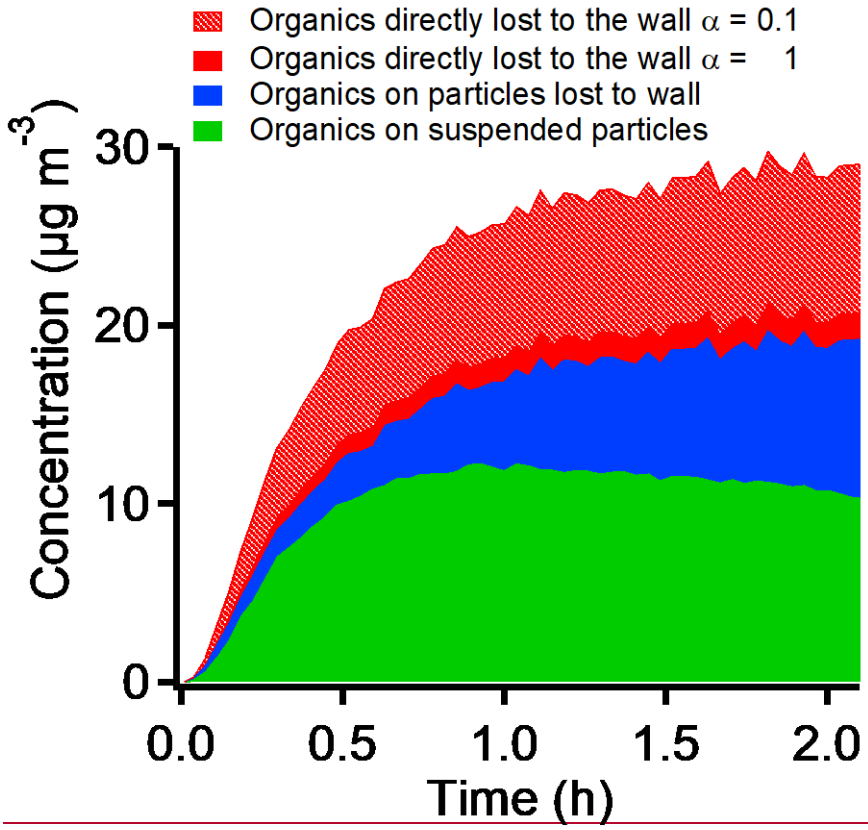

881

882 **Figure 7**. The SOA mass on the suspended particles, lost to chamber wall due to particle wall loss and
883 direct vapor deposition on the chamber wall. When α = 0.1, the SOA mass lost to the chamber wall through
884 the direct vapor deposition may have one third of the total SOA mass. When α = 1, the vapor wall loss may
885 not be significant.

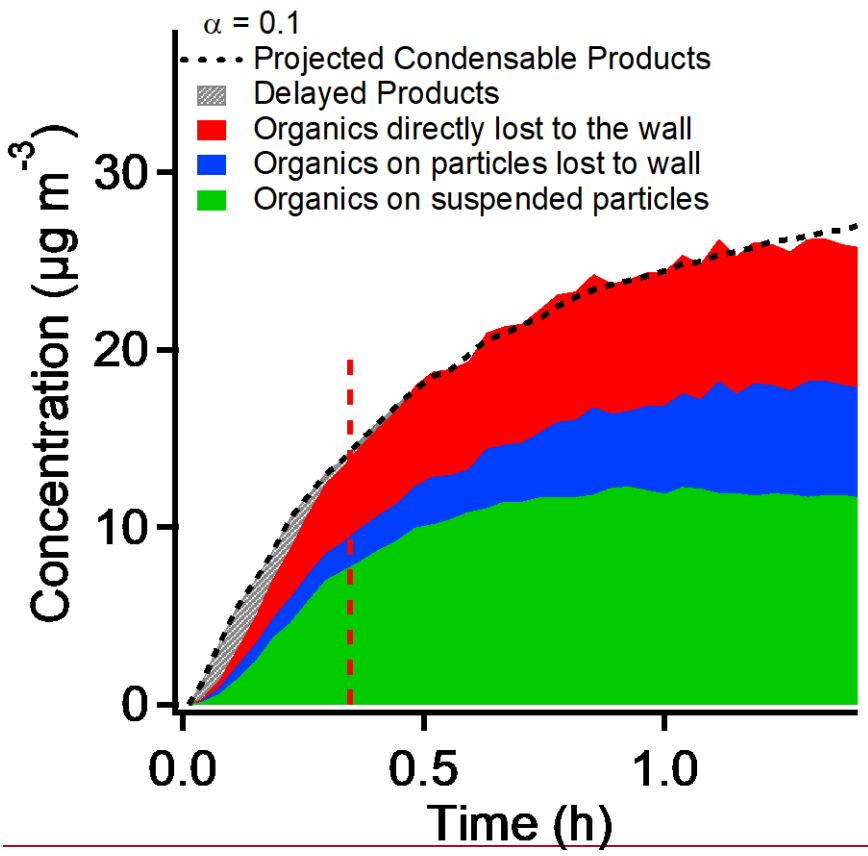
α = 0.1
Projected Condensable Products
Delayed Products
Organics directly lost to the wall
Organics on particles lost to wall
Organics on suspended particles
Concentration (μg m-3)
0
10
20
30
0.0
0.5
1.0
Time (h)

886

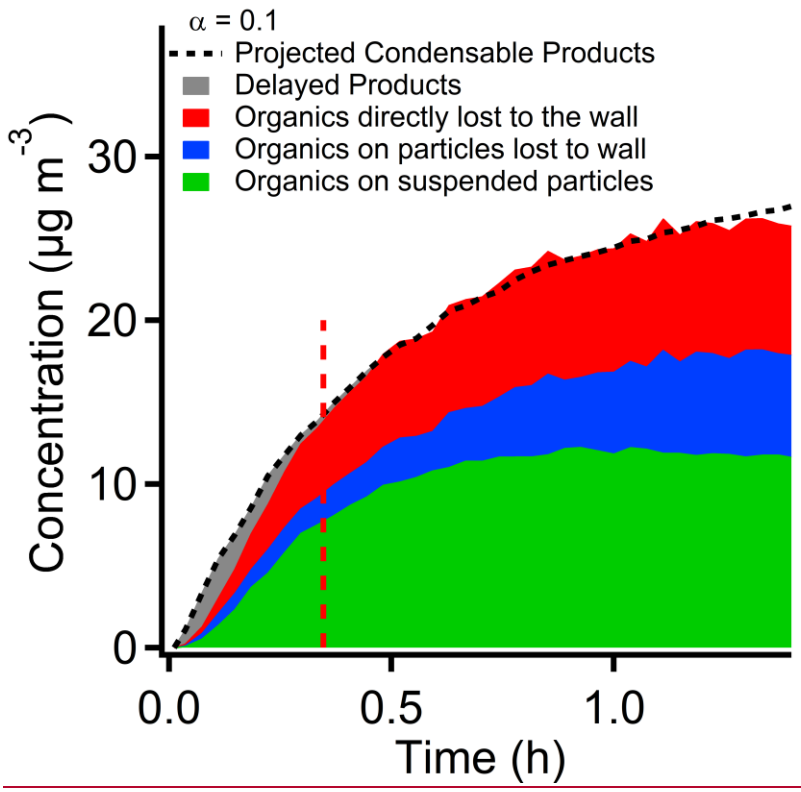

Figure 8. The discrepancy of the observed SOA caused by the condensation delay. The black dash line shows the estimated concentration of condensable vapors from the reacted PD. The dashed area at 0-0.3 hours shows the difference between formed vapors and the observed SOA. This gap may be caused by the diffusion time of vapor molecules to reach the surface of the particles or the chamber walls. This delay may result in a lower measured SOA mass yield at the early stage of the experiment.

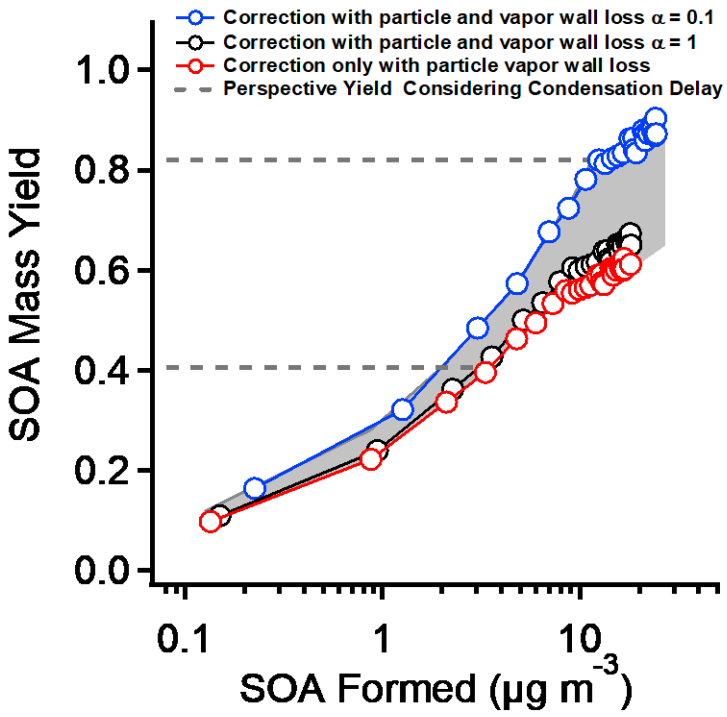

893

894 **Figure 9.** The SOA yield from pinanediol photo-oxidation after correction for particle wall loss and vapor
895 wall loss using three different methods: correction for particle wall-loss only; correction for vapor wall loss
896 with $\alpha = 1$; and correction for vapor wall loss with $\alpha = 0.1$. For the first two methods the mass yields are
897 similar. For the third, when $\alpha = 0.1$, the mass yield is 30% higher than for the other two methods. The
898 horizontal dashed lines indicate the mass yields at a time equal to twice the gas-phase lifetime of vapors
899 due to condensation or wall loss. Before this time (below the lines) the measured SOA yields may be biased
900 low due to the delay between production and condensation to the suspended particles.

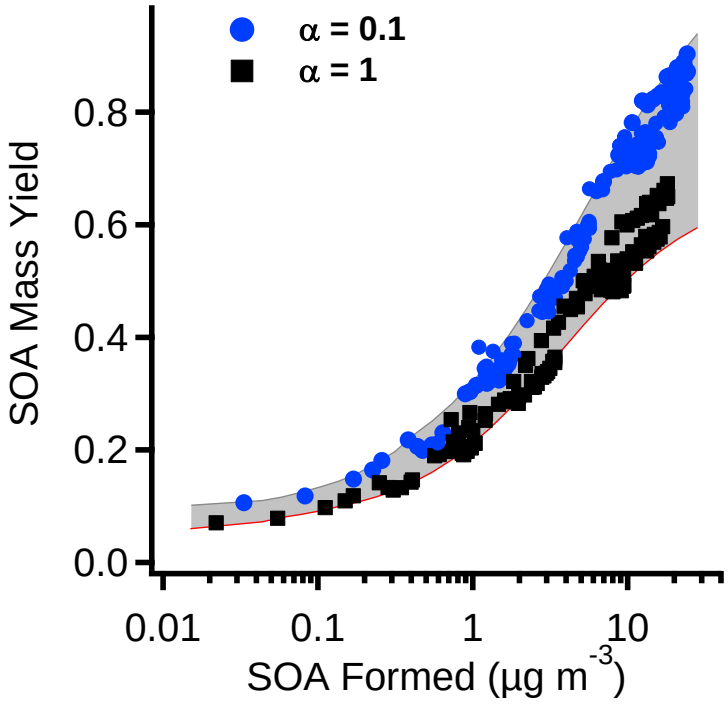

Figure 10. The summary of all the SOA mass yield after correcting both particle and vapor wall loss. The initial PD concentrations are 1,2,4,5, and 6 ppbv.The shade area shows the yield range when α varies from 0.1 to 1.

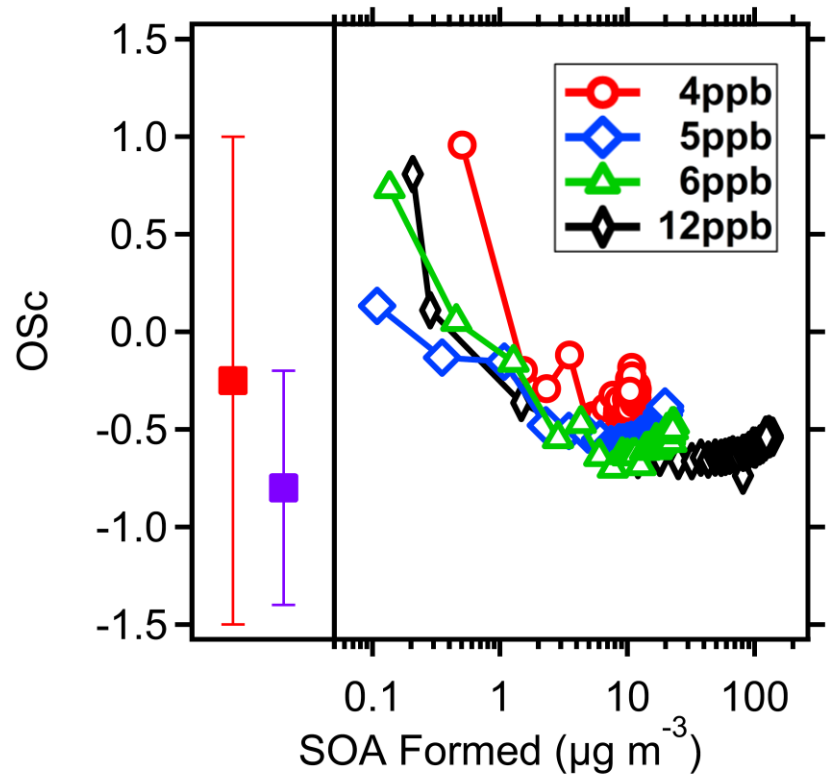

Figure 11. The $\overline{OS}_C$ of the SOA from PD with initial concentrations at 4, 5, 6 and 12 ppb on the right panel. The left panel shows the $\overline{OS}_C$ of the oxidation products from PD in the clusters observed in the CLOUD experiments, which contained 1 (red solid square) and 4 (blue solid square) C_{10} organics. The SOA formed at the very early stage (low yields) shows highly oxidized. The $\overline{OS}_C$ in this study are comparable to the results from the CLOUD experiments.

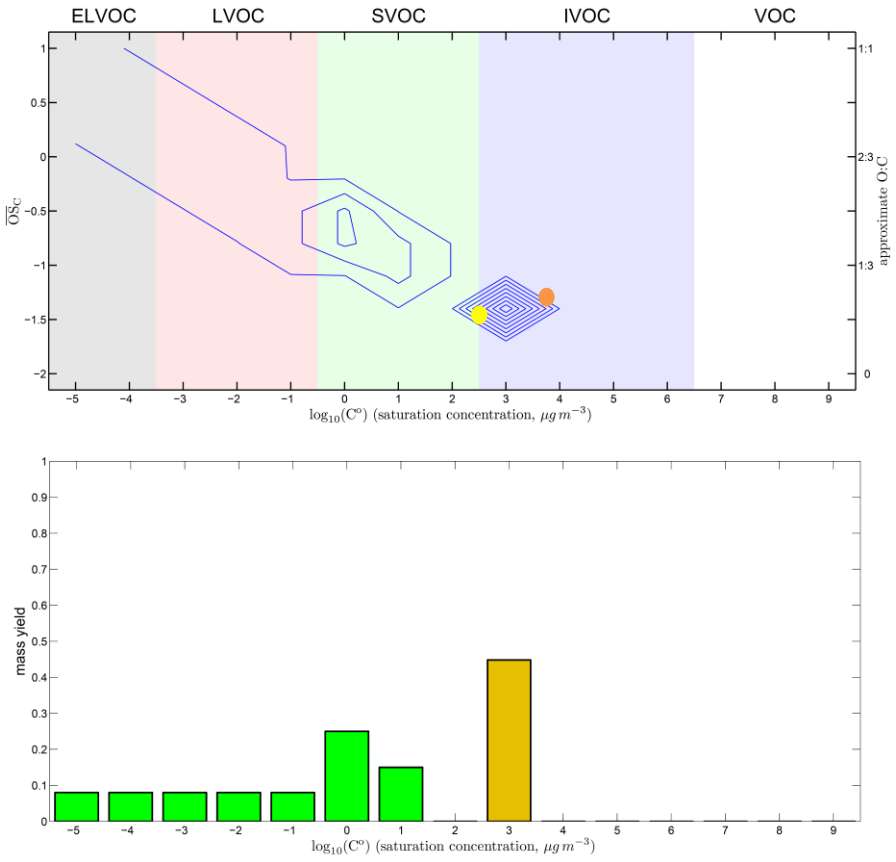

Figure 12. Representation of the oxidation products from PD in the two-dimensional volatility-oxidation space for a mass accommodation coefficient α = 1. We group organics in the broad classes of ELVOCs, LVOCs, SVOCs or IVOCs. The top panel is a 2D representation. PD is shown as a yellow dot. The blue contours show the oxidation products from PD, with higher values indicating higher yields. The lower panel is a 1D consolidation of the 2D product contours, showing the total mass yields in each volatility bin. The major products spread toward the upper left from PD, with increased oxidation state and decreased volatility. The products near to the upper left corner, in the ELVOC region, may contribute to new-particle formation observed in the CLOUD experiments. They constitute around 15% of the total SOA mass. Some products may undergo fragmentation or functional group change, such as converting an alcohol group to a carbonyl group, as with oxy-pinocamphone, which is shown in orange.

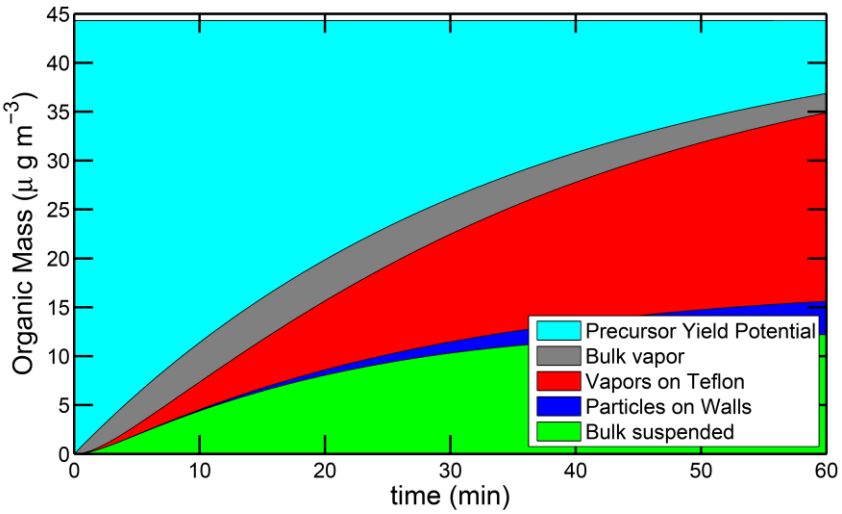

Figure 13. Dynamical simulation of the SOA production from 6 ppb of PD with a mass accommodation coefficient α=1. The simulation treats five different reservoirs: unreacted precursor, vapors, suspended particles, deposited particles, and sorption to teflon, as shown in the legend. The simulation reproduces the SOA observed on the suspended particles.

Supplement of

Secondary organic aerosol production from pinanediol, a semi-volatile surrogate for first-generation oxidation products of monoterpenes

Penglin Ye[a], Yunliang Zhao, Wayne K. Chuang, Allen L. Robinson, Neil M. Donahue[*]

Center for Atmospheric Particle Studies, Carnegie Mellon University, 5000 Forbes Avenue, Pittsburgh, Pennsylvania 15213, United States

[a]now at: Aerodyne Research Inc, Billerica, MA 01821, USA / Nanjing DiLu Scientific Instrument Inc, Nanjing, 210036, China

[*]*Correspondence to:* nmd@andrew.cmu.edu

Phone: (412) 268-4415

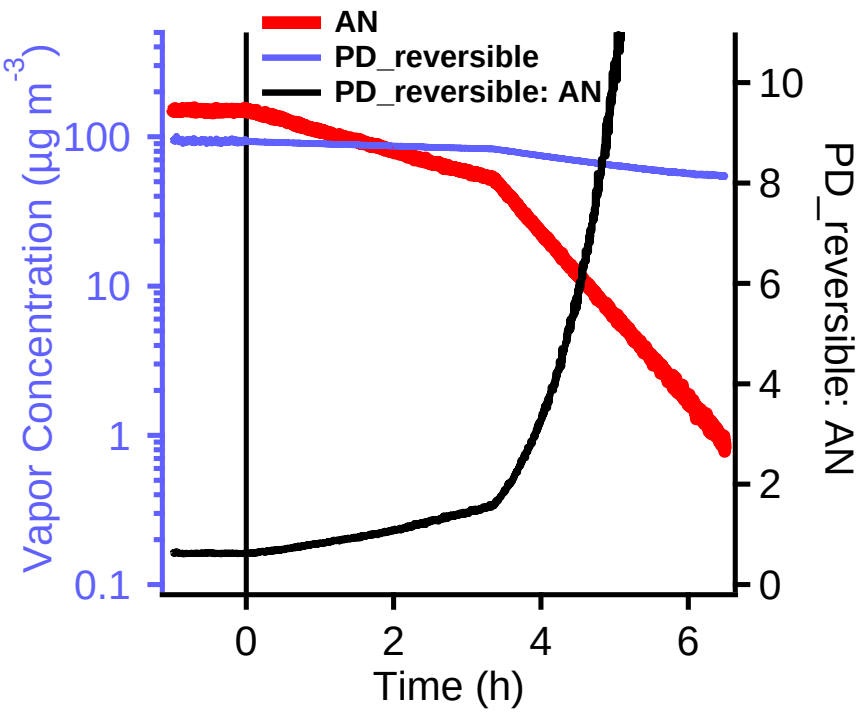

~~Figure S1.~~ ~~The~~ ~~predicted~~ ~~PD~~ ~~concentra~~ ~~tion~~ ~~change~~ ~~during the~~ ~~dilution~~ ~~when~~ ~~consideri~~

Formatted: Right: 5.93", Line spacing: Double

~~ng the~~
~~depositio~~
~~n of PD~~
~~on the~~
~~Teflon~~
~~chamber~~
~~walls as~~
~~reversible~~
~~partitioni~~
~~ng. The~~
~~decrease~~
~~of the~~
~~predicted~~
~~PD~~
~~concentra~~
~~tion~~
~~should be~~
~~slower~~
~~than the~~
~~decrease~~
~~of AN.~~
~~The ratio~~
~~of the~~
~~predicted~~
~~PD to AN~~
~~concentra~~
~~tion~~
~~should~~

~~keep~~

~~increasin~~

~~g.~~

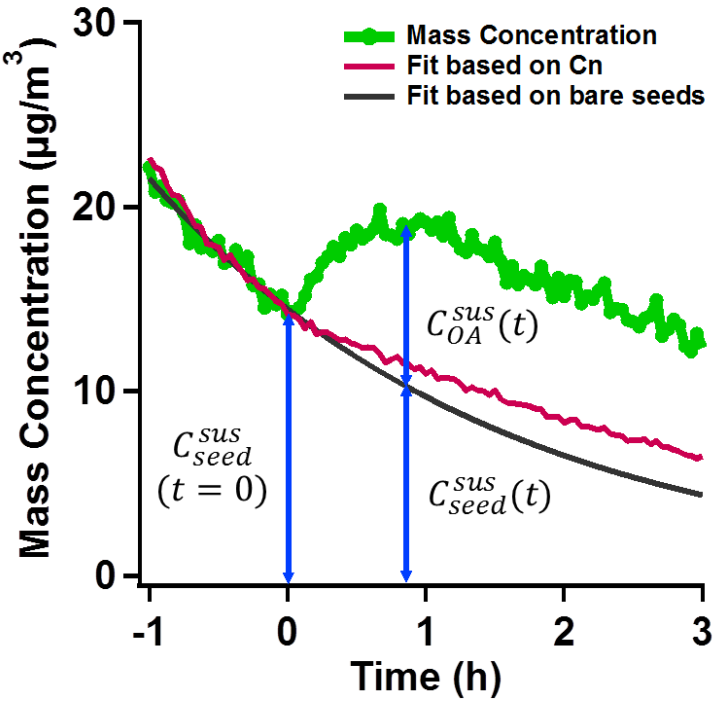

Figure S12. The particle wall loss correction using method 2 and 3. In method 2, $C_{seed}^{sus}(t)$ was determined by applying an exponential function to fit the decay of the pure ammonium sulfate seeds and extrapolate it to the whole experiments (black). $C_{seed}^{sus}(t)$ was also calculated by scaling the total particle number concentration, C_n with the average particle mass in method 3 (red). $C_{SOA}^{sus}(t)$ is the difference between the total particle mass concentration with the $C_{seed}^{sus}(t)$. $C_{seed}^{sus}(t)$ and $C_{SOA}^{sus}(t)$ were both corrected with their densities, 1.78 and 1.4 g cm^{-3}, respectively.

Formatted: Font: Bold

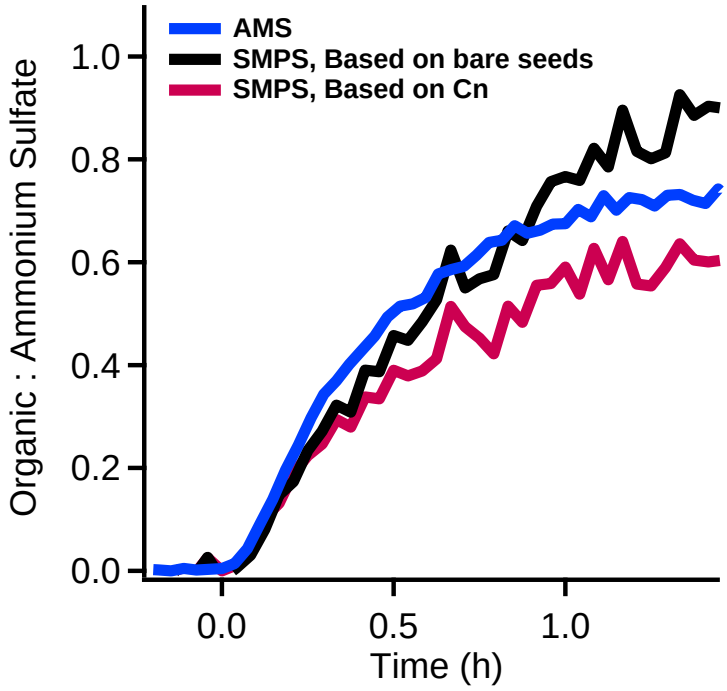

Figure S23. The ratio of organic to ammonium sulfate seed calculated from three methods, directly from AMS measurement in Method 1 (blue), determining the ammonium sulfate seed mass by fitting the decay of the pure seeds and extrapolating it to the whole experiments in Method 2 (black), or by scaling the total particle number concentration, C_n by the average particle mass in method 3 (red). The ratios from all three methods match well with each other. So we only focused on the HR-AMS data to do the particle wall loss correction.

Formatted: Font: Bold

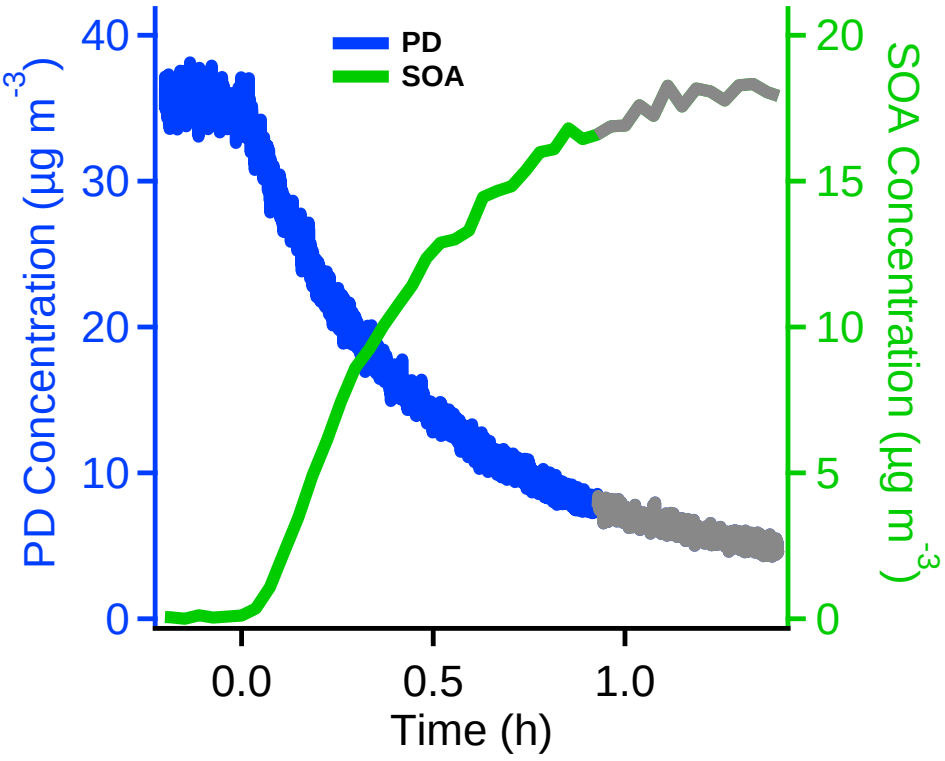

Figure S34. The temporal depletion of PD and formation of SOA. Around 80% of PD were reacted in the first hour. The gray part (less than 22% of its initial value) was not used when calculating the SOA mass yields.

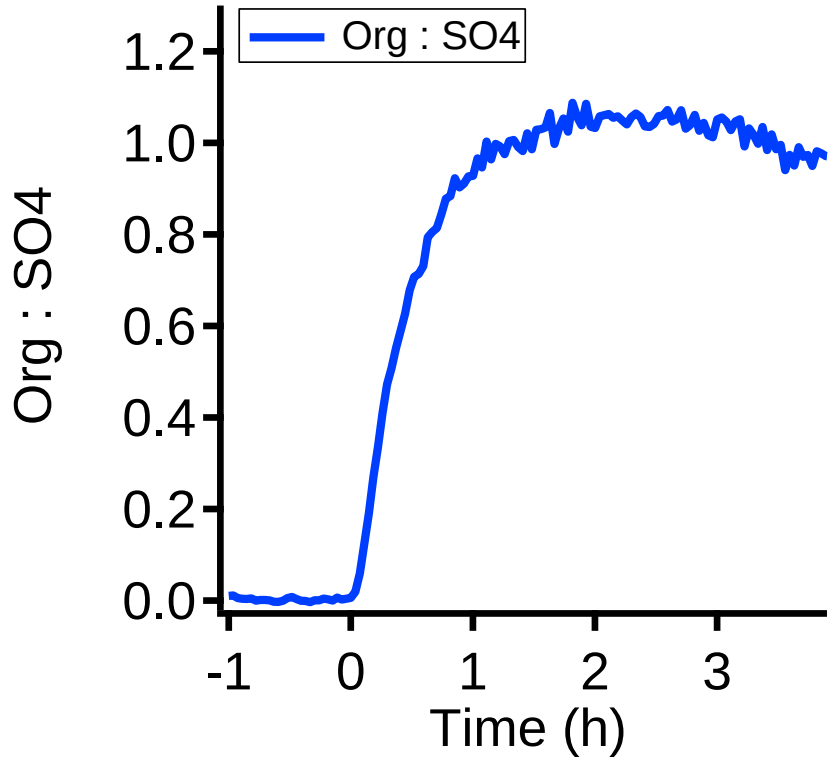

Figure S45. The change of the ratio of organic to sulfate mass from HRAMS measurement. The slight decrease after 2 hours indicated the mass loss from the particles. The may be due to the vapor wall loss which triggers the evaporation of the organics on the particles.

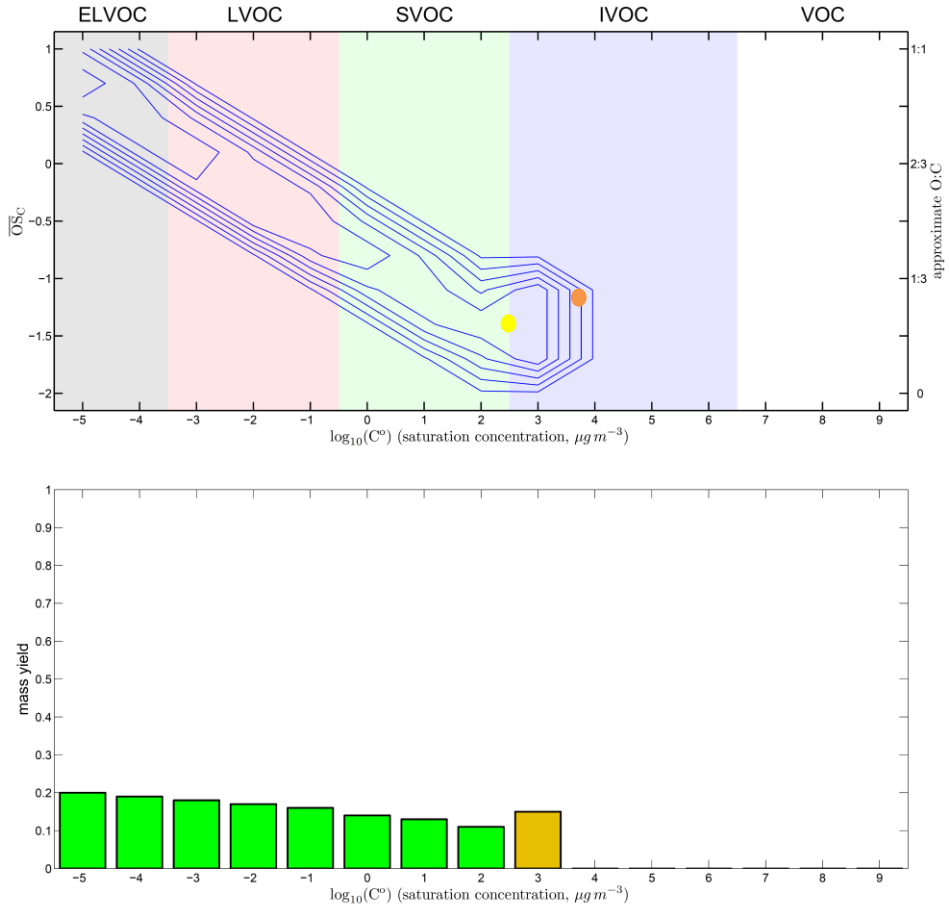

Figure S5~~6~~. Representation of the oxidation products from PD in the two-dimensional volatility-oxidation space when mass accomendation α equals to 0.1. We group organics in the broad classes of ELVOCs, LVOCs, SVOCs or IVOCs. The top panel is a 2D representation. PD is shown as a yellow dot. The blue contours show the oxidation products from PD, with higher values indicating higher yields. The lower panel is a 1D consolidation of the 2D product contours, showing the total mass yields. The major products move to the top left and show more oxidized and less volatile. In this case, ELVOC and LVOC contribute to around 60% of total aerosol mass. ELVOCs and LVOCs usually have very high or unit mass accommodation coefficient, which contradict to the assumption, α equals to 0.1. So α equals to 0.1 may not be the proper value for the SOA studied here.

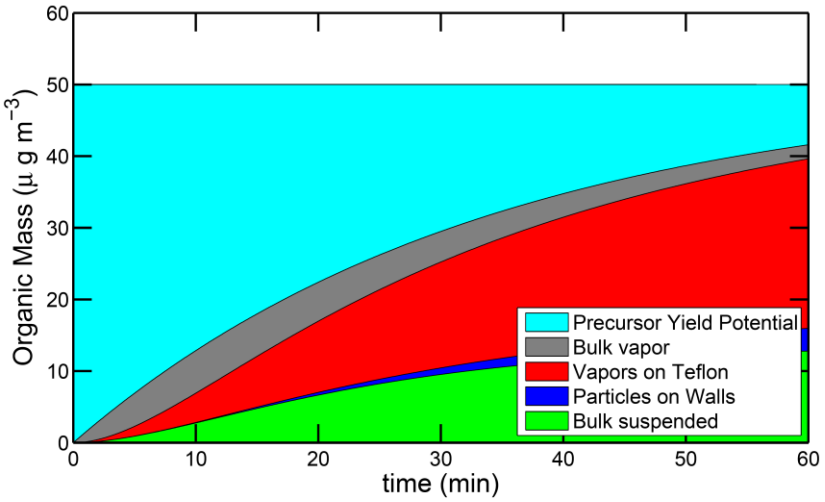

Figure S~~6~~7. Dynamical simulation of the SOA production from 6ppb PD with mass accomendation coefficient α=0.1. The simulation treats five different reservoirs: unreacted precursor, vapors, suspended particles, deposited particles, and sorption to teflon, as shown in the legend.